

ผลของการเติมโลหะออกไซด์ตัวที่สองต่อสมบัติการชอบน้ำของฟิล์มบางไทเทเนียมไดออกไซด์



นายณัฐพงศ์ สอนสะอาด

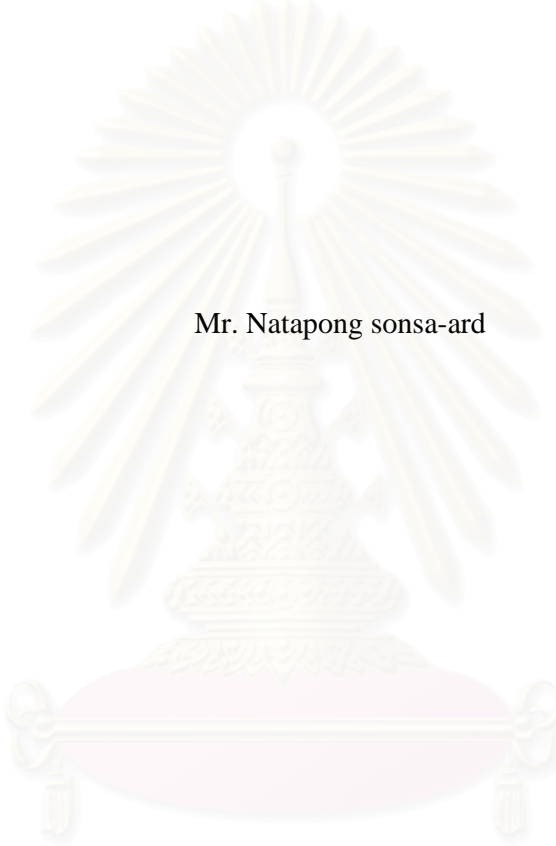
สถาบันวิทยบริการ
วิทยานิพนธ์นี้เป็นส่วนหนึ่งของการศึกษาตามหลักสูตรปริญญาวิศวกรรมศาสตรมหาบัณฑิต
จุฬาลงกรณ์มหาวิทยาลัย
สาขาวิชาวิศวกรรมเคมี ภาควิชาวิศวกรรมเคมี

คณะวิศวกรรมศาสตร์ จุฬาลงกรณ์มหาวิทยาลัย

ปีการศึกษา 2550

ลิขสิทธิ์ของจุฬาลงกรณ์มหาวิทยาลัย

EFFECT OF ADDITION OF SECOND METAL OXIDE ON HYDROPHILIC
PROPERTY OF TiO_2 THIN FILM



Mr. Natapong sonsa-ard

สถาบันวิทยบริการ
จุฬาลงกรณ์มหาวิทยาลัย

A Thesis Submitted in Partial Fulfilment of the Requirements
for the Degree of Master of Engineering Program in Chemical Engineering

Department of Chemical Engineering

Faculty of Engineering

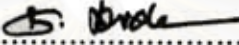
Chulalongkorn University

Academic Year 2007

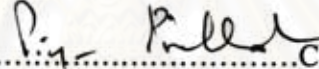
Copyright of Chulalongkorn University


Thesis Title EFFECT OF ADDITION OF SECOND METAL OXIDE ON
HYDROPHILIC PROPERTY OF TiO₂ THIN FILM
By Mr. Natapong Sonsa-ard
Field of study Chemical Engineering
Thesis Advisor Akawat Sirisuk, Ph.D.

Accepted by the Faculty of Engineering, Chulalongkorn University in Partial
Fulfillment of the Requirements for the Master's Degree



.....Dean of the Faculty of Engineering
(Associate Professor Boonsom Lerdhirunwong, Dr.Ing.)


THESIS COMMITTEE


.....Chairman
(Professor Piyasan Praserttham, Dr.Ing.)


.....Thesis Advisor
(Akawat Sirisuk, Ph.D.)


..... Member
(Assistant Professor Bunjerd Jongsomjit, Ph.D.)


.....Member
(Associate Professor Muenduen Phisalaphong, Ph.D.)


.....External Member
(Assistant Professor Okorn Mekasuwandumrong, Ph.D.)

ณัฐพงศ์ สอนสะอาด : ผลของการเติมโลหะออกไซด์ตัวที่สองต่อสมบัติการชอบน้ำของฟิล์มบางไทเทเนียมไดออกไซด์ (EFFECT OF ADDITION OF SECOND METAL OXIDE ON HYDROPHILIC PROPERTY OF TiO_2 THIN FILM) อ. ที่ปรึกษา: คร.อัศววัฒน์ ศิริสุข, 67 หน้า

ไทเทเนียมไดออกไซด์และโลหะออกไซด์ตัวที่สอง คือ ซิงค์ออกไซด์, เซอร์โคเนียมไดออกไซด์, และ เฟอร์ริกออกไซด์ ถูกเตรียมได้โดยวิธีโซล-เจล ไทเทเนียมไดออกไซด์โซลถูกผสมกับโซลของโลหะออกไซด์ตัวที่สอง และปรับปริมาณโลหะออกไซด์ตัวที่สองให้ได้ในช่วง 0-10 โมลเปอร์เซ็นต์ โซลของโลหะออกไซด์ถูกเคลือบบนกระจกสไลด์ โดยวิธีการพ่นฝอยแบบอุลตราโซนิก กระจกสไลด์ที่เคลือบแล้วจะถูกเผาในบรรยากาศที่อุณหภูมิ 350 องศาเซลเซียส เป็นเวลา 2 ชั่วโมง สมบัติการชอบน้ำของฟิล์มบางถูกวัดด้วยเครื่องมือวัดมุมสัมผัสของหยดน้ำ การเติมเซอร์โคเนียมไดออกไซด์หรือซิงค์ออกไซด์ ลงไปอย่างเหมาะสมจะช่วยปรับปรุงสมบัติการชอบน้ำของฟิล์มบางไทเทเนียมไดออกไซด์ ซึ่งสังเกตได้จากอัตราการลดลงที่รวดเร็วของมุมสัมผัสของหยดน้ำในขณะที่ฉายแสงอัลตราไวโอเล็ต การเพิ่มขึ้นของสมบัติการชอบน้ำของฟิล์มบางอาจมีผลมาจากปริมาณ Ti^{3+} และ ความเป็นกรดของพื้นผิวไทเทเนียมไดออกไซด์ นอกจากนี้การเติมซิงค์ออกไซด์ หรือเซอร์โคเนียมไดออกไซด์ลงไป ในไทเทเนียมไดออกไซด์ เป็นการเพิ่มสมบัติในการคงสภาพสมบัติการชอบน้ำของพื้นผิวภายหลังจากการหยุดการฉายแสงอัลตราไวโอเล็ตให้ดียิ่งขึ้น การเติมเฟอร์ริกออกไซด์ลงในฟิล์มบางไทเทเนียมไดออกไซด์ไม่มีผลในการเพิ่มคุณสมบัติการชอบน้ำของฟิล์มบางไทเทเนียมไดออกไซด์

ภาควิชา.....วิศวกรรมเคมี.....
สาขาวิชา.....วิศวกรรมเคมี.....
ปีการศึกษา..... 2550.....

ลายมือชื่อนิสิต.....ณัฐพงศ์ สอนสะอาด.....
ลายมือชื่ออาจารย์ที่ปรึกษา.....อัศววัฒน์ ศิริสุข.....

4970294621 : MAJOR CHEMICAL ENGINEERING

KEY WORD: TITANIA / THINFILM / SUPERHYDROPHILIC PROPERTY

NATAPONG SONSA-ARD: EFFECT OF ADDITION OF SECOND METAL OXIDE ON HYDROPHILIC PROPERTY OF TiO_2 THIN FILM. THESIS ADVISOR: AKAWAT SIRISUK, Ph.D., 67 pp.

Titanium dioxide (TiO_2) and other metal oxides, i.e., ZnO , ZrO_2 , and Fe_2O_3 , were synthesized using sol-gel methods. Then TiO_2 sol was mixed with the sol of another metal oxide so as to obtain the content of the second metal oxide in the range of 0 to 10 mol%. The mixed oxide sols were coated on glass slides using ultrasonic spray coater. The coated slides were calcined at $350\text{ }^\circ\text{C}$ for two hours. The hydrophilic property of thin films was measured using contact angle measurement. The addition of ZnO or ZrO_2 to TiO_2 in an appropriate amount could enhance the hydrophilic property of the mixed oxide thin films, as seen in the faster rate of decrease of contact angle towards a saturated value upon exposure to ultraviolet irradiation. The enhancement of the hydrophilic property of the film could be attributed to increases in the amounts of Ti^{3+} and acid site present on the surface of TiO_2 . Furthermore, addition of ZnO or ZrO_2 to TiO_2 also improved the ability of thin films to retain hydrophilicity after removal of ultraviolet irradiation. Fe_2O_3 was also added to TiO_2 thin film but did not improve hydrophilicity of the thin films.

สถาบันวิทยบริการ
จุฬาลงกรณ์มหาวิทยาลัย

Department Chemical Engineering

Student's signature Natapong Somsa-ard

Field of study Chemical Engineering

Advisor's signature Akawat Sirisuk

Academic Year 2007

ACKNOWLEDGEMENTS

This dissertation would not have been possible to complete without the support of the following individuals. Firstly, I would like to express my greatest gratitude to my advisor, Dr. Akawat Sirisuk, for his invaluable guidance during the course of this work, and I am also very grateful to Professor Piyasan Prasertdam, for his kind supervision over this thesis. Special thanks to Professor Piyasarn Prasertdam, as the chairman, Assistant Professor Muenduen Phisalaphong, Assistant Professor Bunjerd Jongsomjit and Assistant Professor Okorn Mekasuwandumrong, members of the thesis committee for their kind cooperation.

The financial supports from Commission on Higher Education, the Thailand Reserch Fund (TRF), TJTTP-JBIC, and Graduate School of Chulalongkorn University are also gratefully acknowledged.

Many thanks for kind suggestions and useful help to Mr. Kongkiat Suriye and many friends at Center of Excellence on Catalysis and Catalytic Reaction Engineering who always provide the encouragement and assistance along the thesis study.

Finally, I also would like to dedicate this thesis to my parents and my sister who have always been the source of my support and encouragement.

สถาบันวิทยบริการ
จุฬาลงกรณ์มหาวิทยาลัย

CONTENTS

	Page
ABSTRACT (IN THAI).....	iv
ABSTRACT (IN ENGLISH).....	v
ACKNOWLEDGEMENTS.....	vi
CONTENTS.....	vii
LIST OF TABLES.....	x
LIST OF FIGURES.....	xi
CHAPTER	
I INTRODUCTION.....	1
II LITERATURE REVIEWS.....	3
2.1 Effect of titanium dioxide phase structure.....	3
2.2 Effect of Ti ³⁺ surface defect.....	3
2.3 Effect of hydroxyl group on the surface.....	4
2.4 Effect of surface acidity.....	4
2.5 Effect of metal oxide of photocatalytic activity.....	5
III THEORY.....	6
3.1 Information on titanium dioxide.....	6
3.1.1 Physical and Chemical Properties.....	6
3.1.2 Applications of titanium dioxide.....	10
3.2 Sol-gel method.....	11
3.3 Theory of photo-induced hydrophilicity.....	11
3.4 Relationship between Photocatalysis and hydrophilic properties.....	15
3.5 Wettability and contact angle.....	15
IV MATERIALS AND METHODS.....	17
4.1 Preparation of titanium dioxide thin films.....	17
4.1.1 Preparation of titanium dioxide sol.....	17
4.1.2 Preparation of zirconium dioxide sol.....	18
4.1.3 Preparation of zinc oxide sol.....	18
4.1.4 Preparation of iron oxide.....	18
4.1.5 Preparation of mixed oxide sol.....	19
4.1.6 Preparation of metal oxide thin films.....	19

	Page
4.2 Characterization of metal oxide thin films.....	19
4.2.1 X-ray diffractometry (XRD).....	19
4.2.2 Electron spin resonance (ESR).....	20
4.2.3 Temperature-programmed desorption (NH ₃ -TPD).....	20
4.2.4 Bet Single point surface area (BET).....	21
4.2.5 Atomic force microscope (AFM).....	21
4.3 Measurement of photo-induced hydrophilicity of TiO ₂	21
V RESULTS AND DISCUSSION.....	22
5.1 Effect of addition of ZnO to TiO ₂ thin film.....	22
5.1.1 Phase structures of ZnO/TiO ₂	22
5.1.2 Surface morphology of ZnO/TiO ₂ thin film.....	24
5.1.3 Specific surface area of ZnO/TiO ₂	26
5.1.4 Temperature Programmed Desorption (TPD).....	27
5.1.5 ESR results.....	28
5.1.6 Photo-induced hydrophilicity.....	30
5.1.7 Ability to sustain hydrophilicity of ZnO/TiO ₂ film after removal of UV irradiation.....	30
5.2 Effect of addition of ZrO ₂ to TiO ₂ thin film.....	32
5.2.1 Phase structures of ZrO ₂ /TiO ₂	32
5.2.2 Surface morphology of ZrO ₂ /TiO ₂ thin film.....	34
5.2.3 Specific surface area of ZrO ₂ /TiO ₂	36
5.2.4 Temperature Programmed Desorption (TPD).....	37
5.2.5 ESR results.....	38
5.2.6 Photo-induced hydrophilicity.....	40
5.2.7 Ability to sustain hydrophilicity of ZrO ₂ /TiO ₂ film after removal of UV irradiation.....	40
5.3 Effect of addition of Fe ₂ O ₃ to TiO ₂ thin film.....	42
5.3.1 Phase structures of Fe ₂ O ₃ /TiO ₂	42
5.3.2 Surface morphology of Fe ₂ O ₃ /TiO ₂ thin film.....	44
5.3.3 Specific surface area of Fe ₂ O ₃ /TiO ₂	46
5.3.4 Temperature Programmed Desorption (TPD).....	47
5.3.5 ESR results.....	48

5.3.6 Photo-induced hydrophilicity.....	49
5.3.7 Ability to sustain hydrophilicity of Fe ₂ O ₃ /TiO ₂ film after removal of UV irradiation.....	49
VI CONCLUSIONS AND RECOMMENDATIONS.....	51
6.1 Conclusions.....	51
6.2 Recommendations for future studies.....	51
REFERENCES.....	52
APPENDICES.....	55
APPENDIX A: CALCULATION OF THE CRYSTALLITE SIZE.....	56
APPENDIX B: CALCULATION OF THE CONTACT ANGLE.....	59
APPENDIX C: DATA AND CALCULATION OF ACID SITE..	60
APPENDIX D: DETERMINATION OF Ti ³⁺ SURFACE DEFECT FROM ESR MEASUREMENT.....	62
APPENDIX E: DETERMINATION OF LATTICE PARAMETERS OF TITANIUM DIOXIDE.....	63
LIST OF PUBLICATION.....	66
VITA.....	67

สถาบันวิทยบริการ
จุฬาลงกรณ์มหาวิทยาลัย

LIST OF TABLES

Table	Page
3.1 Comparison of rutile, brookite and anatase.....	7
5.1 Crystallite size of anatase in ZnO/TiO ₂ with various amount of ZnO, as determined from XRD pattern.....	23
5.2 Grain size and average roughness of ZnO/TiO ₂ thin film as determined from AFM images.....	24
5.3 Specific surface area of ZnO/TiO ₂ with various amount of ZnO.....	26
5.4 Surface acidity of ZnO/TiO ₂ samples as determined from NH ₃ -TPD.....	28
5.5 Amount of Ti ³⁺ surface defect in various ZnO/TiO ₂ films as determined for ESR measurements.....	29
5.6 Crystallite size of anatase in ZrO ₂ /TiO ₂ with various amount of ZrO ₂ , as determined from XRD patterns.....	33
5.7 Grain size and average roughness of ZrO ₂ /TiO ₂ thin film as determined from AFM images.....	34
5.8 Specific surface area of ZrO ₂ /TiO ₂ with various amount of ZrO ₂	36
5.9 Surface of acidity of ZrO ₂ /TiO ₂ samples as determined from NH ₃ -TPD.....	38
5.10 Amount of Ti ³⁺ surface defect in various ZrO ₂ /TiO ₂ films as determined for ESR measurements.....	39
5.11 Crystallite size of anatase in Fe ₂ O ₃ /TiO ₂ with various amount of Fe ₂ O ₃ , as determined from XRD pattern.....	43
5.12 Grain size and average roughness of Fe ₂ O ₃ /TiO ₂ thin film as determined from AFM images.....	44
5.13 Specific surface area of Fe ₂ O ₃ /TiO ₂ with various amount of Fe ₂ O ₃	46
5.14 Surface acidity of Fe ₂ O ₃ /TiO ₂ samples as determined from NH ₃ -TPD.....	47
C.1 Reported total peak area from Micromeritics Chemisorb 2750.....	60
F.1 The 2θ value of (101) plane and (200) plane of ZnO/TiO ₂ in each sample from XRD measurement.....	64
F.2 Summary of lattice parameters and crystal volume from XRD analysis.....	65

LIST OF FIGURES

Figure	Page
3.1 Structure of TiO ₂ anatase (a) and rutile (b).....	9
3.2 Photocatalytic process occurring on an illuminated semiconductor particle	12
3.3 Surface and bulk electron trapping.....	13
3.4 Mechanism of photo-induced hydrophilicity.....	14
3.5 Mechanism of hydrophilic TiO ₂ thin film. TiO ₂ film illuminated by UV light provides surface hydrophilic (a). Then, water can spread over a film thoroughly (b).....	14
3.6 The force balance among the three surface tensions for determining the contact angle.....	16
5.1 XRD patterns of ZnO/TiO ₂ film calcined at 350 °C. The amount of ZnO was varied added.....	23
5.2 AFM images of ZnO/TiO ₂ film surfaces that contained a) 0%, b) 2%, c) 4%, d) 6%, e) 8%, and f) 10% mol of ZnO.....	25
5.3 NH ₃ -TPD peaks of ZnO/TiO ₂ films by various amount of ZnO.....	27
5.4 Show intensity of ZnO/TiO ₂ powder by various amount of ZnO calcined at 350 °C reported from ESR.....	29
5.5 Change in contact angle of water droplet on the surfaces of various ZnO/TiO ₂ films upon exposure to UV irradiation.....	31
5.6 Change in contact angle of water droplet on the surface of various ZnO/TiO ₂ films in the absence of UV irradiation.....	31
5.7 XRD patterns of ZrO ₂ /TiO ₂ film calcined at 350 °C. The amount of ZrO ₂ added was varied.....	33
5.8 AFM images of ZrO ₂ /TiO ₂ film surface that contained a) 0%, b) 2%, c) 4%, d) 6%, e) 8%, and f) 10% mol of ZrO ₂	35
5.9 NH ₃ -TPD peaks of ZrO ₂ /TiO ₂ films by various amount of ZrO ₂	37
5.10 Show intensity of ZrO ₂ /TiO ₂ powder by various amount of ZrO ₂ calcined at 350 °C report from ESR.....	39
5.11 Change in contact angle of water droplet on the surfaces of various ZrO ₂ /TiO ₂ films upon exposure to UV irradiation.....	41

5.12 Change in contact angle of water droplet on the surface of various ZrO ₂ /TiO ₂ films in the absence of UV irradiation.....	41
5.13 XRD patterns of Fe ₂ O ₃ /TiO ₂ film calcined at 350 °C. The amount of Fe ₂ O ₃ was varied added.....	43
5.14 AFM images of Fe ₂ O ₃ /TiO ₂ film surfaces that contained a) 0%, b) 2%, c) 4%, d) 6%, e) 8%, and f) 10% mol of Fe ₂ O ₃	45
5.15 NH ₃ -TPD peaks of Fe ₂ O ₃ /TiO ₂ films by various amount of Fe ₂ O ₃	47
5.16 Results from ESR measurements for various Fe ₂ O ₃ /TiO ₂ samples.....	48
5.17 Change in contact angle of water droplet on the surfaces of various Fe ₂ O ₃ /TiO ₂ films upon exposure to UV irradiation.....	49
5.18 Change in contact angle of water droplet on the surface various Fe ₂ O ₃ /TiO ₂ films in the absence of UV irradiation.....	50
A.1 The 101 diffraction peak of titania for calculation of the crystallite size.....	57
A.2 The plot indicating the value of line broadening due to the equipment. The data were obtained by using alumina as standard.....	58
B.1 The shape and dimension of water droplet.....	59
F.1 Tetragonal crystal structure of titanium dioxide.....	63

CHAPTER I

INTRODUCTION

Titanium dioxide (TiO_2) is widely used in many applications such as photocatalysis, self-cleaning surface, UV absorber, pigment, gas sensor, or coating. TiO_2 film exhibits hydrophilic property when irradiated by UV-light. The photoinduced hydrophilicity of TiO_2 is similar to photocatalytic process. Electron and hole are generated when TiO_2 is exposed to UV irradiation. TiO_2 surface will show hydrophilicity and the contact angle of water becomes zero.

Hydrophilic surface reduces the contact angle of water droplet on the surface to be smaller than 10 degrees. However, this property is not stable. The surface can return to hydrophobic state when being kept away from UV irradiation for an extended period of time.

Several metal oxide such as SiO_2 , Al_2O_3 , ZnO , ZrO_2 , SnO and Fe_2O_3 , were added to TiO_2 in order to increase the photocatalytic activity of TiO_2 (Celik et al., 2006; Guan et al., 2005; Hernandez-Alonso et al., 2006; Kang et al., 2003; Maeda and Hirota, 2006; Sun et al., 2001). There may be a correlation between photocatalytic activity and hydrophilic property of TiO_2 (Guan et al., 2005). Therefore, in this study various metal oxides (i.e., ZrO_2 , Fe_2O_3 , and ZnO) were added to TiO_2 . The effects of addition of the second metal oxide to TiO_2 on hydrophilic property of the modified TiO_2 thin films and their abilities to retain hydrophilicity after removal of UV irradiation were investigated. TiO_2 was synthesized using a sol-gel method. And TiO_2 sol was coated on a substrate using spray coating technique.

The objective of this research is to investigate the effects of addition of the second metal oxide to TiO_2 on the hydrophilic property of the modified TiO_2 thin film.

This thesis is arranged as follows:

Chapter II presents literature reviews of previous works related to this research.

Chapter III explains basic information about titania and also discusses principles of photo-induced hydrophilic properties.

Chapter IV describes synthesis of titania, second metal oxide, and preparation of titania thin film employed in this research and experimental apparatus and setting.

Chapter V presents experimental results and discussion.

Chapter VI presents overall conclusions of this research and recommendations for future research.

สถาบันวิทยบริการ
จุฬาลงกรณ์มหาวิทยาลัย

CHAPTER II

LITERATURE REVIEWS

This chapter presents a survey of literatures pertaining to hydrophilic property of titanium dioxide thin film and the effects of various parameters on such property.

2.1 Effect of titanium dioxide phase structure

Watanabe and coworkers (1999) studied the different plane of rutile single crystal and polycrystalline anatase titanium dioxide. Anatase polycrystalline was prepared by a sol-gel method and coated on a soda lime glass that was coated with a silicon dioxide layer and was fired in air at 500 °C for 20 minutes. The (110) surface of rutile single crystal had bridging oxygen, which was more reactive, but not on the (001) surface. So the rate of decrease in contact angle, saturated contact angle and conversion rate of hydrophilicity to hydrophobicity of (110) surface were better.

Yu and coworkers (2002) studied two different structures of titanium dioxide. They used a reverse micellar and a sol-gel methods to synthesize both mesoporous TiO₂ (MTiO₂) and TiO₂ thin films. TiO₂ thin films were calcined at 500 and 900 °C to obtain two different phase structures: anatase and rutile. The result for both MTiO₂ and TiO₂ indicated that anatase phase was more hydrophilic than rutile phase.

2.2 Effect of Ti³⁺ surface defect

Lee and coworkers (2003) investigated the effect of doping of aluminium (Al), tungsten (W) and both aluminium and tungsten (Al+W) on hydrophilicity of thin film. TiO₂ thin film was coated on soda lime glass and quartz substrate using a dip technique. Then the films were baked at 150 °C and annealed at 500 °C. Doping of either Al or W brought about a slight decrease in contact angle (40° and 25°) after being irradiated for long time, while doping two metal gave rise to

the lowest contact angle (5°). The same trend was observed for both types of substrate. XPS analysis revealed that concentration of Ti^{3+} on TiO_2 surface was a major factor influencing hydrophilicity. The concentrations of Ti^{3+} in undoped, Al-doped, W-doped and Al+W-doped were 58.63%, 46.45%, 57.91 % and 63.81% ($\text{Ti}^{3+}/\text{Ti}^{4+}$), respectively. Furthermore, hydrophilicity of titanium dioxide also depended on traps for electrons or holes and the surface acidity.

2.3 Effect of hydroxyl group on the surface

Jiaguo and Xiujian (2001) studied the effect of surface microstructure on superhydrophilic property of TiO_2 thin film prepared by a sol-gel method. Polyethylene glycol (PEG) was added to improve properties of film. When the amount of PEG increased, pore sizes of the film became larger. The addition of PEG increased the number of surface hydroxyl groups, which resulted in greater hydrophilicity. However, when amount of PEG reached 0.5 g, the contact angle of titania thin film remained unchanged.

Jiaguo and Xiujian (2002) studied the difference between TiO_2 thin films before and after treatment with hydrochloric acid (HCl). Titanium dioxide was coated on a glass substrate and was heated at 500°C for one hour. Then the sample was soaked in 0.2 M HCl for four days. This result showed that thickness of TiO_2 film did not affect superhydrophilicity. Moreover, XPS analysis indicated that hydroxyl group of treated TiO_2 film increased and led to a decrease in the contact angle.

2.4 Effect of surface acidity

Guan and coworkers (2005) investigated the effect of the amount of SiO_2 addition on the photo-generated hydrophilicity of TiO_2 films. Addition of 40 mol% SiO_2 to TiO_2 was most effective for reducing the contact angle of water. The contact angle of water remained low for a long time in dark place. Addition of SiO_2 suppressed the crystal growth of TiO_2 during calcination and enhanced the transmittance of the composite films. SiO_2 and TiO_2 formed single oxide particles in the films, but a part of complex oxide may be formed. Ti–O–Si bonds increased the acidity, which induced an increase in the hydroxyl content in the composite films.

2.5 Effect of metal oxide of photocatalytic activity

Kang and coworker (2003) studied the nanoparticle of two $\text{Fe}_x\text{O}_y/\text{TiO}_2$'s with high photocatalytic activities. The nanoparticles were obtained through a hydrothermal treatment and an impregnation method. $\text{Fe}_x\text{O}_y/\text{TiO}_2$ particles that were prepared by a hydrothermal treatment had higher hydrophilic property and increase acidity on the surface compared to the impregnation method because Fe components were well incorporated into the TiO_2 anatase structure. But decomposition of CHCl_3 on the $\text{Fe}_x\text{O}_y/\text{TiO}_2$ catalyst was not largely enhanced compared to pure TiO_2 .

Maeda and Hirota (2006) studied bilayer structures of Ti film on SnO_x film prepared by magnetron sputtering. In the $\text{TiO}_x/\text{SnO}_x$ composite films, the SnO_x formed impurity levels in the TiO_x bandgap and simultaneously prevented crystallization of TiO_2 . These impurity levels were considered to play a role in visible-light absorption. Photocatalytic activities under visible light were observed only in the $\text{TiO}_x/\text{SnO}_x$ composite film.

Alonso and coworkers (2006) studied the characteristics of $\text{TiO}_2\text{-ZrO}_2$ thin films supported on glass for the photocatalytic removal of VOCs. Acidic sols of different composition (ZrO_2 , TiO_2 and Ti-Zr mixed oxides) were investigated. The results indicated that, for the same Zr content, the photoactivity of the films containing binary metal oxides was slightly higher than that of the solid solution. In contrast, specific surface area seemed to have little influence on the performance of the thin films.

Sun and coworkers (2001) investigated the photoinduced surface wettability conversion reactions of ZnO and TiO_2 thin films by means of water contact angle measurement. UV illumination turned both surfaces to highly hydrophilic with water contact angles smaller than 10° . The similar behaviors of wettability conversion observed on ZnO and TiO_2 surfaces suggested that they followed a similar conversion mechanism. Preferential adsorption of water molecules on the photogenerated surface defective sites was ascribed to the formation of highly hydrophilic ZnO and TiO_2 surfaces.

CHAPTER III

THEORY

This chapter consists of four main sections. Section 3.1 discusses properties and applications of titanium dioxide. Synthesis of such materials by a sol-gel method is described in Section 3.2. Details on photo-induced hydrophilicity processes are discussed in Section 3.3. Definition of contact angle and classification of hydrophilicity and hydrophobicity described in Section 3.4.

3.1 Information on titanium dioxide

This section discusses properties and applications of titanium dioxide. This material was employed to coat glass substrates to be tested for photo-induced hydrophilicity.

3.1.1 Physical and Chemical Properties (Othmer, 1991; Fujishima et al., 1999)

Titanium dioxide may take on any of the following three crystal structures: anatase, which tends to be more stable at low temperature; brookite, which is usually found only in minerals; and rutile, which tends to be more stable at higher temperatures and thus is sometimes found in igneous rock.

Anatase generally shows a higher photocatalytic activity than the other types of titanium dioxide. Comparison of some physical properties of rutile and anatase is shown in Table 3.1.

Table 3.1 Comparison of rutile, brookite and anatase. [Othmer, 1991 and Fujishima et al., 1999).

Properties	Anatase	Brookite	Rutile
Crystal structure	Tetragonal	Orthorhombic	Tetragonal
Optical	Uniaxial, negative	Biaxial, positive	Uniaxial, negative
Density, g/cm ³	3.9	4.0	4.23
Harness, Mohs scale	5 ^{1/2} – 6	5 ^{1/2} – 6	7 – 7 ^{1/2}
Unit cell	D _{4h} ¹⁹ .4TiO ₂	D _{2h} ¹⁵ .8TiO ₂	D _{4h} ¹² .3TiO ₂
Dimension, nm			
a	0.3758	0.9166	0.4584
b	-	0.5436	-
c	0.9514	0.5135	2.953
Refractive index	2.52	-	2.52
Permittivity	31	-	114
Melting point	changes to rutile at high temperature	-	1858°C

The reason that anatase is more photoactive than rutile may lie in the differences in their so-called energy band structures. The band gap energy of a semiconductor is the minimum energy of light required to make the material electrically conductive or, in other words, to get the electrons excited enough to get moving. The band gap energy of anatase is 3.2 eV, which corresponds to UV light with wavelength of 388 nanometers, while the band gap energy for the rutile type is 3.0 eV, corresponding to violet light that has a wavelength of 413 nanometers. The level of the conduction band for anatase is 0.2 eV higher than that for rutile. In more technical terminology, the band gap energy for a semiconductor indicates the

minimum energy of light necessary to produce electrons in the conduction band (CB) and give rise to electrical conductivity (photoconductivity) and “holes,” which are actually the absence of electrons, in the valence band (VB). These holes can react with water to produce the highly reactive hydroxyl radical ($\bullet\text{OH}$). Both holes and hydroxyl radicals can oxidize most organic materials.

The VB energies for both anatase and rutile are very low in the energy. Consequently, the VB holes (and the hydroxyl radicals) have great oxidizing power. The CB energy for rutile is close to the potential required to electrolytically reduce water to hydrogen gas. The CB energy for anatase is higher in the energy, meaning that it has higher reducing power. Therefore, anatase can drive the very important reaction involving the electrolytic reduction of molecular oxygen (O_2) to superoxide ($\bullet\text{O}_2^-$).

Although anatase and rutile are both tetragonal, they do not have the same crystal structures. Anatase exists in near-regular octahedral while rutile forms slender prismatic crystal. Rutile is the thermally stable form and is one of the two most important ores of titanium.

The three forms of titanium (IV) oxide have been prepared in laboratories but only rutile, the thermally stable form, has been obtained in the form of transparent large single crystal. The transformation from anatase to rutile is accompanied by the evolution of ca. 12.6 kJ/mol (3.01 kcal/mol), but the rate of transformation is greatly affected by temperature the presence of other substance which may either catalyze or inhibit the reaction. The lowest temperature at which conversion of anatase to rutile takes place at a measurable rate is around 700 °C, but this is not a transition temperature. The change is not reversible since ΔG for the change from anatase to rutile is always negative. Brookite has been produced by heating amorphous titanium (IV) oxide, which is prepared from an alkyl titanate or sodium titanate, with sodium or potassium hydroxide in an autoclave at 200 to 600 °C for several days. The important commercial forms of titanium (IV) oxide are anatase and rutile, and they can readily be distinguished by X-ray diffraction spectrometry.

Since both anatase and rutile are tetragonal, they are both anisotropic, and their physical properties, e.g. refractive index, vary according to the direction relative to the crystal axes. In most applications of these substances, the distinction between crystallographic direction is lost because of the random orientation of large numbers of small particles, and only average values of the properties are significant.

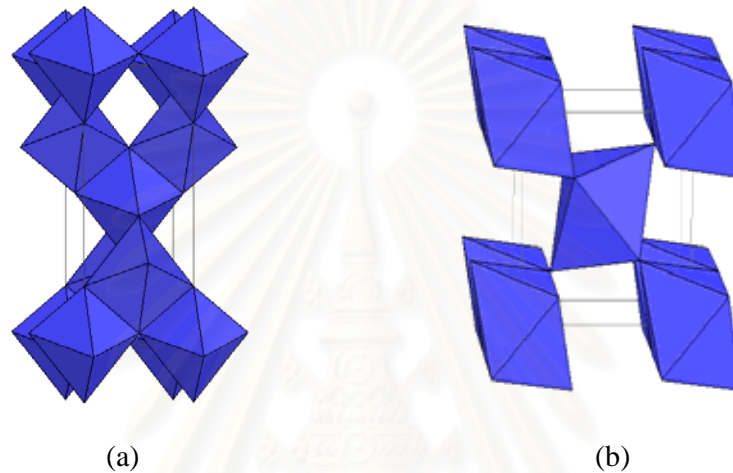


Fig 3.1 Structure of TiO₂ anatase (a) and rutile (b) phase

Measurement of physical properties, in which the crystallographic directions are taken into account, may be made for both natural and synthetic rutile, natural anatase crystals, and natural brookite crystals. Measurements of the refractive index of titanium (IV) oxide must be made by using a crystal that is suitably orientated with respect to the crystallographic axis as a prism in a spectrometer. Crystals of suitable size of all three modifications occur naturally and have been studied. However, rutile is the only form that can be obtained in large artificial crystals from melts. The refractive index of rutile is 2.75. The dielectric constant of rutile varies with direction in the crystal and with any variation from the stoichiometric formula, TiO₂ and an average value for rutile in powder form is 114. The dielectric constant of anatase powder is 48.

Titanium dioxide is thermally stable (mp 1855 °C) and very resistant to chemical attack. When it is heated strongly under vacuum, there is a slight loss of oxygen corresponding to a change in composition to $\text{TiO}_{1.97}$. The product is dark blue but reverts to the original white color when it is heated in air.

Hydrogen and carbon monoxide reduce titanium dioxide only partially at high temperatures, yielding lower oxides or mixtures of carbide and lower oxides. At ca. 2000 °C and under vacuum, carbon reduces titanium dioxide to titanium carbide. Reduction by metal, e.g., Na, K, Ca, and Mg, is not complete. Chlorination is only possible if a reducing agent is present.

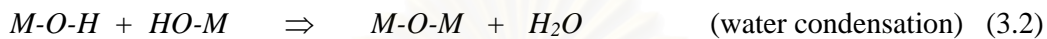
3.1.2 Applications of titanium dioxide

Titanium dioxide is one of the most basic materials in our daily life. Titanium dioxide has been widely used in a variety of paints, plastics, paper, inks, fibers, cosmetics, sunscreens, and foodstuffs.

Naturally, the type of titanium dioxide that is used as a pigment is different from that used as a photocatalyst. The photocatalytic technology is becoming more and more attractive to industries today because environmental pollution has been recognized as a serious problem that needs to be addressed immediately. Various applications in which research and development activities involving titanium dioxide have been investigated, such as fog-proof, anti-bacterial, anti-viral, fungicidal, anti-soiling, self-cleaning, deodorizing, air purification, anti-cancer, water treatment, and water purification.

3.2 Sol-gel method (Fu et al., 1996; Su et al., 2004)

This process occurs in liquid solution of organometallic precursors such as tetraethyl orthosilicate, zirconium propoxide and titanium isopropoxide, which, by means of hydrolysis and condensation reaction, lead to the formation of sol.



A typical example of a sol-gel method is the addition of metal alkoxides to water. The alkoxides are hydrolyzed giving the oxide as a colloidal product.

The sol is made of solid particles of a diameter of few hundred nanometers suspending in a liquid phase. After that, the particles condense into gel, in which solid macromolecules are immersed in a liquid phase. Drying the gel at low temperature (25-100 °C) produces porous solid matrices or xerogels. To obtain a final product, the gel is heated. This heat treatment serves several purposes, *i.e.*, to remove solvent, to decompose anions such as alkoxides or carbonates to give oxides, to rearrange of the structure of the solid, and to allow crystallization to occur.

Using a sol-gel method, one can easily control a stoichiometry of solid solution and a homogeneous distribution of nanoparticles and metal oxides. In addition, the advantages are that the metal oxides are prepared easily at room temperature and high purity can be obtained.

3.3 Theory of photo-induced hydrophilicity (Fujishima et al., 2000)

The primary process involving photo-induced hydrophilicity occurs upon irradiation of a semiconductor. A semiconductor is characterized by an electronic band structure, in which the highest occupied energy band, or valence band, and the lowest empty band, conduction band, are separated by a band gap. The magnitude of the energy of band gap between the electronically populated valence

band and the largely vacant conduction band governs the extent of thermal population of the conduction band in its intrinsic state. The band gap defines the wavelength sensitivity of the semiconductor to irradiation. A photon of energy higher than or equal to the band gap energy is absorbed by a semiconductor particle. Then an electron from the valence band is promoted to the conduction band with simultaneous generation of an electronic vacancy or "hole" (h^+) in the valence band. This process is photoexcitation of electrons. Figure 3.2 shows the photocatalytic process occurring on an irradiated semiconductor particle.

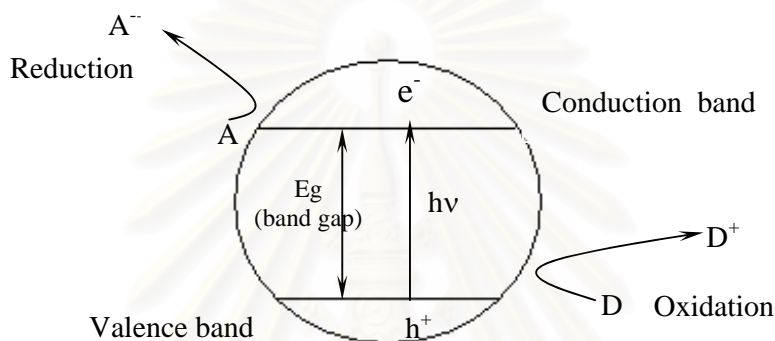
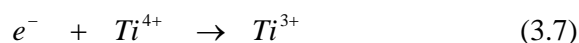
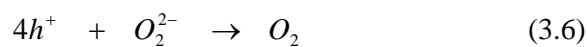
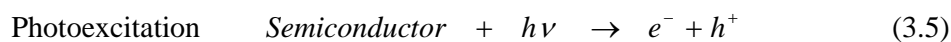
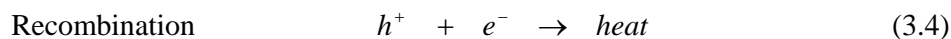


Figure 3.2 Photocatalytic process occurring on an illuminated semiconductor particle (Litter, 1999).

In most materials that are electrically conductive, i.e., metals, two types of charge carriers, electrons (e^-) and holes (h^+), immediately recombine on the surface or the bulk of particle in a few nanoseconds and the accompanying energy is dissipated as heat (see Equation 3.4). On semiconductor such as titanium dioxide, however, the charge carriers survive for longer periods of time to allow themselves to be trapped in surface states where they can react with donor (D) or acceptor (A) species adsorbed or close to the surface of the particle, according to Equations 3.5, 3.6, and 3.7 (Litter, 1999). Subsequently, oxidation and reduction can be initiated.



Electron-hole recombination processes may be suppressed by bulk and surface traps. In Figure 3.3, the energy levels of the bulk and surface traps fall within the band gap. The surface and bulk traps are localized, and the electrons trapped in such states are thus associated with a particular site on the surface or in the bulk of the solid. The population of bulk and surface traps depend on two factors, namely, the decrease in entropy that occur when electrons are trapped, and the difference in relative energy between the traps and the bottom of the conduction band.

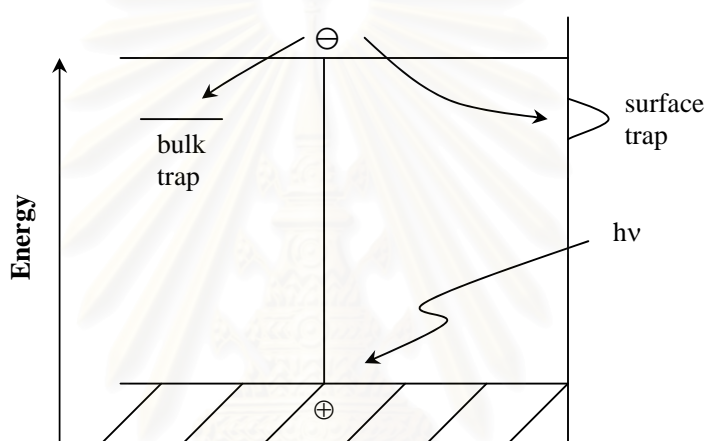


Figure 3.3 Surface and bulk electron trapping (Linsebigler et al., 1995).

The photogenerated electrons reduce Ti (IV) cations to Ti (III) state, and the holes oxidize the O_2^{2-} anions. Then, oxygen atoms are ejected, creating oxygen vacancies (Figure 3.4). Water molecules can then replace these oxygen vacancies, producing chemisorbed hydroxyl groups (Figure 3.5a). These hydroxyl groups can adsorb and spread water to create superhydrophilicity (Figure 3.5b). The longer the surface is illuminated with UV light, the smaller the contact angle for water becomes. After 30 minutes or so under a moderate intensity UV light source, the contact angle approaches zero, meaning that water has a tendency to spread perfectly across the surface.

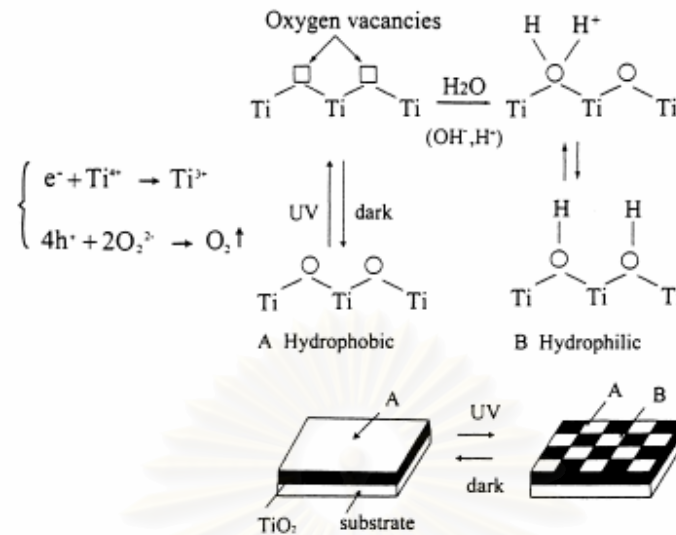


Figure 3.4 Mechanism of photo-induced hydrophilicity (Fujishima et al., 2000)

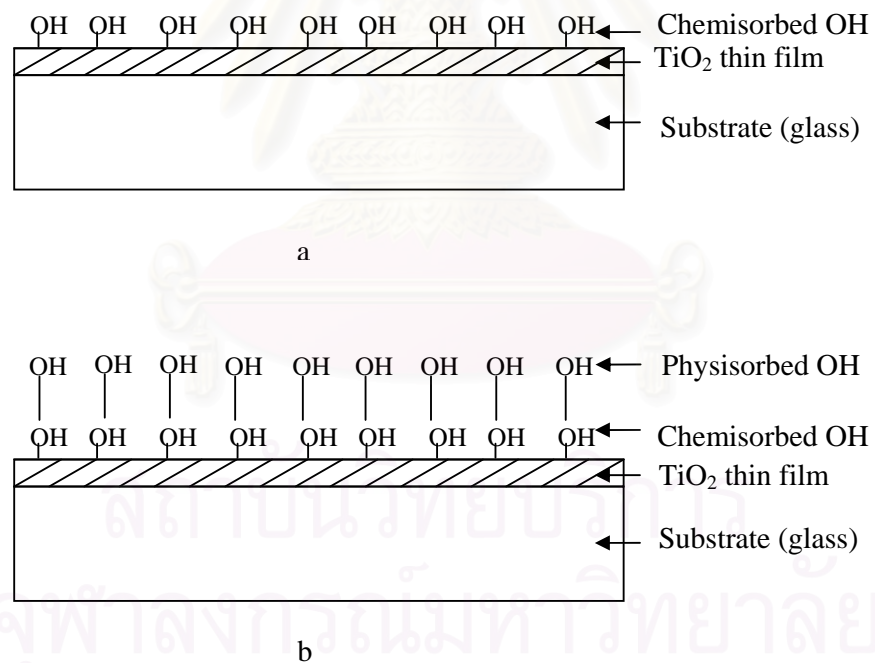


Figure 3.5 Mechanism of hydrophilic TiO₂ thin film. TiO₂ film illuminated by UV light provides surface hydrophilic (a). Then, water can spread over a film thoroughly (b).

3.4 Relationship between photocatalytic and hydrophilic properties.

In spite of the different mechanisms of photocatalytic effect and hydrophilic effect, the correlation between the two effects is obvious. The dependence resembles that of photo-induced hydrophilicity which suggests that the photo-induced hydrophilicity of the film closely relates to the photocatalytic removal of organic substances from the film surface. The synergetic effect of photocatalysis and hydrophilicity can be explained as follows. Because more OH groups can be adsorbed on the surface due to hydrophilicity, the photocatalytic activity is enhanced. So hydrophilicity can improve photocatalysis. On the other hand, the film surface can adsorb contaminated compounds which tend to turn the hydrophilic surface to hydrophobic surface. Photocatalysis can decompose the organic compounds deposit on the surface to H₂O, CO₂ and other small organic compounds to restore hydrophilicity. From this point, photocatalysis can improve hydrophilicity and sustain this characteristic for a long time.

3.5 Wettability and contact angle (De Gennes, 1985)

The contact angle is the angle at which a liquid/vapor interface meets the solid surface. The contact angle is specific for any given system and is determined by the interactions across the three interfaces. Most often the concept is illustrated with a small liquid droplet resting on a flat horizontal solid surface (see Figure 3.6). Ideally, the droplet should be as small as possible because the force of gravity, for example, can actually change the above-mentioned angle. The shape of the droplet is determined by Young equation in Equation 3.8.

$$\cos \theta = \frac{\sigma_{sa} - \sigma_{sl}}{\sigma_{la}} \quad (3.8)$$

Where θ = contact angle

σ_{sa} = surface tension between solid and ambient atmosphere

σ_{sl} = surface tension between solid and liquid

σ_{la} = surface tension between liquid and ambient atmosphere

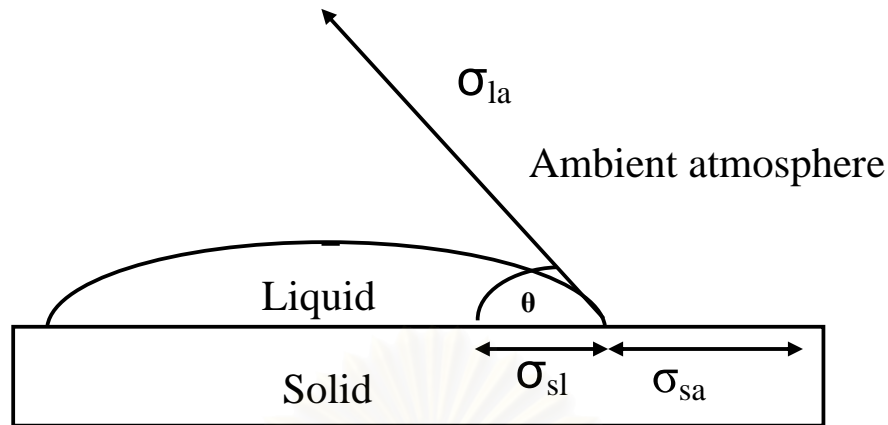


Figure 3.6 The force balance among the three surface tensions for determining the contact angle.

The theoretical description of contact angle arises from the consideration of a thermodynamic equilibrium between the three phases: the liquid phase of the droplet (l), the solid phase of the substrate (s) and the gas/vapor phase of the ambient (a) (see Figure 3.6). At equilibrium, the chemical potential in the three phases should be equal. It is convenient to frame the discussion in terms of the interfacial energies or surface tension.

The wettability of substrate can be classified by the contact angle into four regions.

1. $\theta < 5^\circ$: Water can spread completely over the substrate surface. This state is called “superhydrophilic”.
2. $5^\circ < \theta < 90^\circ$: The surface chemistry allows these materials to be wetted forming a water film or coating on their surface. This state is called “hydrophilic”.
3. $90^\circ < \theta < 150^\circ$: Materials have little or no tendency to adsorb water and water tends to bead on their surfaces. This state is called “hydrophobic”.
4. $\theta > 150^\circ$: Water droplets simply rest on the surface, without actually wetting to any significant extent. This state is called “superhydrophobic”.

CHAPTER IV

MATERIALS AND METHODS

4.1 Preparation of titanium dioxide thin films

This section describes methods for preparation of titanium dioxide thin film using sol-gel processes.

4.1.1 Preparation of titanium dioxide sol

Titanium dioxide was prepared using a sol-gel method, and titanium isopropoxide (Aldrich Chemical, Milwaukee, WI) was employed as a precursor. First, 7.33 ml of 70% nitric acid (Asia Pacific Specialty Chemicals Limited) was added to 1000 ml of distilled water. While the acidic solution was stirred, 83.5 ml of titanium isopropoxide was added slowly. The suspension was stirred continuously at room temperature for about 3 days until clear sol was obtained. After that, the sol was dialyzed in a cellulose membrane with a molecular weight cutoff of 3500 (Spectrum Companies, Gardena, CA). Prior to use, the dialysis tubing was washed in an aqueous solution of 0.001M EDTA and 2% sodium hydrogen carbonate. The wash solution was prepared by dissolving 0.372 grams of EDTA (Asia Pacific Specialty Chemicals Limited) and 43 grams of sodium hydrogen carbonate powder, 99.93% (Fisher Scientific Chemical) in one liter of distilled water. Dialysis tubing was cut into sections of 32 cm in length and was submerged in the wash solution. Then the membrane was heated to 80 °C and held there for 30 minutes while simultaneously being stirred. After the solution was cooled to room temperature, the tubing was washed with distilled water by immersing in one liter of fresh distilled water while being stirred continuously, and being heated to 80 °C. The tubing was rinsed one more time and was stored in distilled water at 4 °C until needed.

4.1.2 Preparation of zirconium dioxide sol

Zirconium dioxide was prepared using a sol-gel method, and zirconium propoxide (Aldrich Chemical, Milwaukee, WI) was employed as a precursor. First, 2.2 ml of 70% nitric acid (Asia Pacific Specialty Chemicals Limited) was added to 105.2 ml of distilled water. While the acidic solution was stirred, 7.6 ml of zirconium propoxide was added slowly. A white precipitate immediately formed and produced a cloudy suspension during the addition. The suspension was then continuously for 3-4 days to obtain the clear sol.

4.1.3 Preparation of zinc oxide sol

Zinc oxide were prepared by a sol-gel method. As a precursor, 10 g zinc acetate dehydrate (Aldrich Chemical, Milwaukee, WI) was first dissolved into 100 ml ethanol (Merck, Darmstadt, Germany) at 60 °C while stirred. After stirring for one hour, a clear and homogeneous sol was obtained.

4.1.4 Preparation of iron oxide

Iron oxide was prepared using a sol-gel method and ferric nitrate Nonahydrate (Fluka Chemie, USA) was employed as a precursor. First, 83.3 g of ferric nitrate nonahydrate was dissolved in Milli-Q H₂O to produce 250 ml of 0.83 M Fe(NO₃)₃ solution. The solution was filtered through a glass micro-fiber filter (Whatman GF/F). Separately, 40 g of NaOH was dissolved in Milli-Q water to give 200 ml of 5 M NaOH solution. Ferric nitrate solution into a Quorpak glass jar with TFE-lined lids. Then 8.32 ml of 5 M NaOH was added rapidly to the iron solution, while the solution was being stirred. The solution had an OH/Fe ratio of 2.0. Precipitation occurred rapidly and redissolved in about 40 minutes, after which the pH is approximately 1.5.

4.1.5 Preparation of mixed oxide sol

Titanium dioxide sol was mixed with the sol of the second metal oxide by stirring. The amount of second metal oxide was varied from 2 -10 mole percentage. The mixed sol was placed in dialysis membrane tubing. Then the tubing containing the mixed sol was submerged in distilled water using a ratio of 100 ml of mixed sol per 700 ml of distilled water. The water was changed daily for 3-4 days until the pH of the water reached 3.5 to remove solvents. The resulting product was dialyzed mixed sol. The mixed sol was kept at low temperature.

4.1.6 Preparation of metal oxide thin films

Metal oxide thin films were prepared using an ultrasonic spray coater. The substrate was clean glass slide (Sail Brand). The amount of mixed oxide sol sprayed on the glass slide was controlled to be the same for every sample. The films were dried at 100 °C for two hours and were then calcined under air at 350 °C. The heating rate was 10 °C/min and holding time in the furnace was two hours. The films were kept in the dark for two weeks to ascertain complete hydrophobicity of the films.

4.2 Characterization of metal oxide thin films

In order to determine physical and chemical properties of thin films, various characterization techniques were employed. Such techniques are discussed in this section.

4.2.1 X-ray diffractometry (XRD)

XRD was employed to identify crystal phase and crystallinity of thin film. The equipment used was a SIEMENS D 5000 X-ray diffractometer with CuK_α radiation with Ni filter in the 2θ range of 20-60° with a resolution of 0.02°. The sample was metal oxide thin film on glass slides.

4.2.2 Electron spin resonance (ESR)

Electron spin resonance was carried out using a JEOL JES-RE2X electron spin resonance spectrometer to determine the amount of Ti^{3+} surface defect in metal oxide powders. Recorded spectra were scanned and converted to a g-value, according to a Mn^{2+} marker. The amount of samples used was approximately 0.3 grams.

4.2.3 Temperature-programmed desorption (NH_3 -TPD)

Temperature programmed desorption (TPD) using NH_3 as a probe molecule performed in a Micromeritic ChemiSorb 2750 automated system attached with ChemiSoft TPx software. The amount of NH_3 adsorbed on the surface was determined by a thermal conductivity detector.

Approximately 0.2 grams of sample was placed in a quartz tube in a temperature-controlled furnace. Helium gas with a flow rate of 15 ml/min was fed through sample. The sample was heated from room temperature to 350 °C with a heating rate of 10 °C/min and held for two hours to remove moisture. Then the sample was cooled down to 30 °C. After that, 15 vol% NH_3 in helium flowed through sample at a flow rate of 15 ml/min instead of helium, and held for one hour. Subsequently, helium gas was fed through the sample for two hours. Finally, the sample was heated from 30 °C to 850 °C with a heating rate of 10 °C/min. The signal from this step was recorded every one second and stored on a microcomputer.

สถาบันวิทยบริการ
จุฬาลงกรณ์มหาวิทยาลัย

4.2.4 Nitrogen physisorption

Specific surface area was measured through nitrogen adsorption in a continuous flow method at liquid nitrogen temperature. A mixture of nitrogen and helium was employed as the carrier gas using Micromeritics ChemiSorb 2750 Pulse Chemisorption System instrument. The sample was thermally treated at 200 °C for 1 hour before each measurement.

4.2.5 Atomic force microscope (AFM)

The surface morphology was characterized with atomic force microscopy (AFM measurements), using a MultiMode (Digital Instruments) microscope operated in the tapping mode, in air, and room temperature.

4.3 Measurement of photo-induced hydrophilicity of TiO₂

Photo-induced hydrophilicity of TiO₂ was determined by the contact angle measurement. For each TiO₂-coated glass, initial contact angle value was measured before irradiation with 15 W black light blue fluorescent bulbs. A water droplet was dropped from the syringe designed for control of droplet volume. The volume of a water droplet was approximately 3.0 ml. A sample was placed on a stage and the stage was raised to meet the syringe. When water was in contact with a sample, the camera captured the projection picture. A water contact angle was then calculated using trigonometry formula. The equipment was a TANTEC. After that, the samples were exposed to UV irradiation in the black box. The sample was removed every 10 minutes to measure the contact angle until the angle was below 10 degrees.

CHAPTER V

RESULT AND DISCUSSION

This chapter presents the results and discussion on effect of addition of the second metal oxide on properties of TiO₂ thin films.

5.1 Effect of addition of ZnO to TiO₂ thin film.

5.1.1 Phase structures of ZnO/TiO₂

The bulk crystalline phases of samples were determined using X-ray diffractometer (XRD). ZnO/TiO₂ samples were prepared via a sol-gel method. The amount of ZnO added was 2, 4, 6, 8, and 10 mol%. Then the films were calcined at 350 °C for two hours under atmospheres.

From the XRD patterns of ZnO/TiO₂ powder were calcined at 350 °C (see Figure 5.1), the dominant peak of anatase were observed at 2θ of about 25.2°, 37.9°, 47.8°, and 53.8°, which corresponded to the index of (101), (004), (200), and (105) plane, respectively. The weak peak at 2θ of 30.9° was assigned to brookite phase of TiO₂. XRD peaks that belong to rutile phase were not detected at this temperature. Even when the ZnO content was as high as 10 mol%, none of XRD peaks associated with ZnO were detected in any samples. Moreover, inspection of intensities of anatase peaks in the sample, which correlated with crystallinity of the sample, indicated that addition of ZnO led to smaller diffraction peaks, thereby reducing the crystallinity of TiO₂. When amount of ZnO was increased, the crystallinity of thin film was decreased further. The sample with 10 mol% of ZnO possessed the lowest crystallinity when compared to the other samples.

Average crystallite size of anatase was determined from XRD pattern using the Scherrer equation. The results are listed in Table 5.1. Addition of ZnO to TiO₂ appeared to increase the average crystallite size of anatase only slightly.

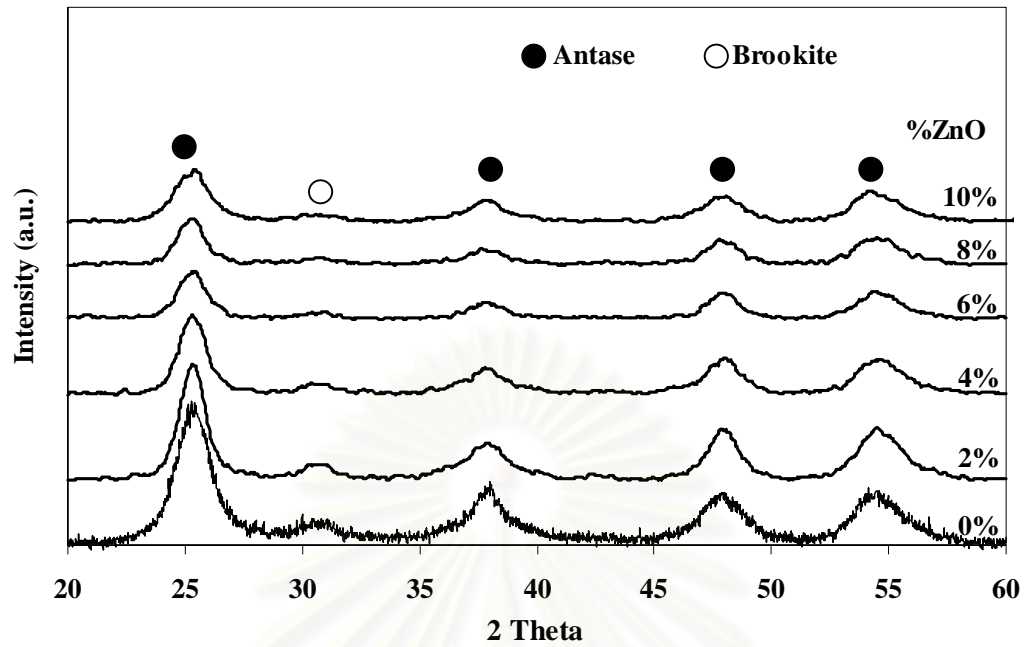


Figure 5.1 XRD patterns of ZnO/TiO₂ film calcined at 350 °C. The amount of ZnO was varied added.

Table 5.1 Crystallite size of anatase in ZnO/TiO₂ with various amount of ZnO, as determined from XRD pattern.

Amount of ZnO (mol%)	Crystallite size (nm)
0	4.5
2	6.3
4	6.1
6	5.9
8	5.9
10	4.8

5.1.2 Surface morphology of ZnO/TiO₂ thin film

Figure 5.2 shows the surface topography images of ZnO/TiO₂ thin film coated on glass surfaces. The surface images of ZnO/TiO₂ thin film with 0%, 2%, 4%, 6%, 8%, and 10% mol ZnO are shown in Figures 5.2 (a), (b), (c), (d), (e), and (f), respectively.

Analysis of AFM images suggests that addition of ZnO into TiO₂ increased the grain size of TiO₂. The more ZnO added, the larger the grain size (see Table 5.2). However, the average roughness of the ZnO/TiO₂ film surface appeared not to be effected by the addition of ZnO.

Table 5.2 Grain size and average roughness of ZnO/TiO₂ thin film as determined from AFM images

Amount of ZnO (mol%)	Grain size (nm)	Average roughness from AFM (nm)
0	2.468	2.631
2	1.860	2.052
4	2.284	2.395
6	2.543	2.181
8	2.136	2.253
10	3.346	2.354

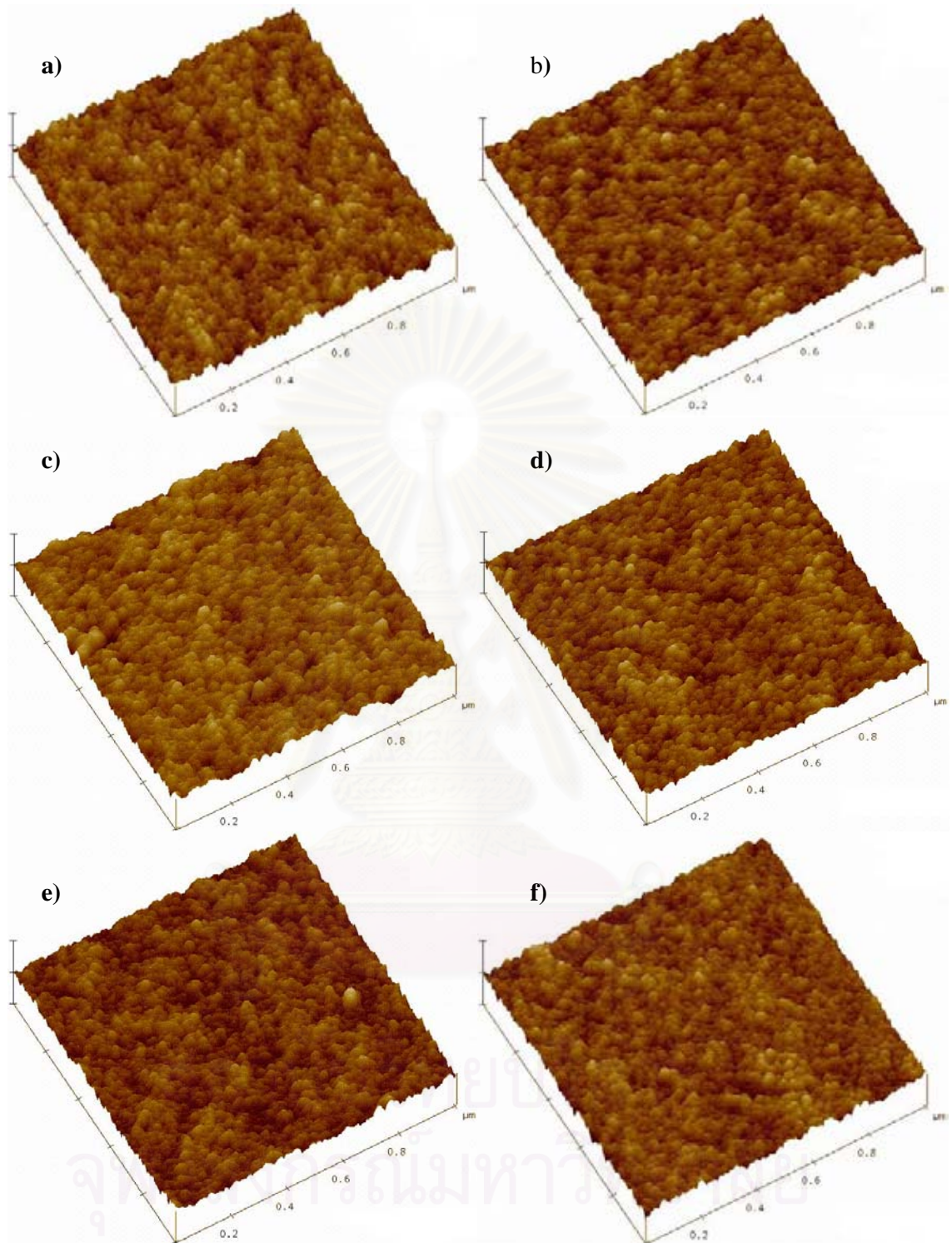


Figure 5.2 AFM images of ZnO/TiO₂ film surfaces that contained a) 0%, b) 2%, c) 4%, d) 6%, e) 8%, and f) 10% mol of ZnO.

5.1.3 Specific surface area of ZnO/TiO₂

The most common procedure for determining surface area of a solid is based on adsorption and condensation of nitrogen at liquid nitrogen temperature using static vacuum procedure. This method is also call BET (Brunauer Emmett Teller) method using nitrogen as the adsorption at 77 K in a Micromeritics Chemisorb 2750 automated system. Specific surface area of ZnO/TiO₂ samples was measured. The samples were dried at 200 °C for one hour in a 30% N₂/He flow prior to BET measurements. The measured BET surface areas of titanium dioxide samples were in the range of 101.2-125.1 m²/g. The surface area went down when the amount of ZnO was increased up to 6 mol%. After that, the surface area increased again (see Table 5.3). These results agreed with the work done by Shijun and coworkers [2004], in which they found that addition of ZnO did not have a significant effect on the specific surface area of the mixed oxide.

Table 5.3 Specific surface area of ZnO/TiO₂ with various amount of ZnO.

Amount of ZnO (mol%)	Specific surface area (m ² /g)
0	125.1
2	123.8
4	120.6
6	101.2
8	111.4
10	123.8

5.1.4 Temperature Programmed Desorption (TPD)

Temperature-programmed desorption using ammonia as a probe molecule was employed to determine the amount of the acid site on ZnO/TiO₂ powders. The results are shown in Table 5.4. Addition of ZnO to TiO₂ increased total number of acid sites, thereby raising the surface acidity of ZnO/TiO₂. The highest surface acidity was achieved in ZnO/TiO₂ samples that contained 4-6 mol% ZnO (see Figure 5.3).

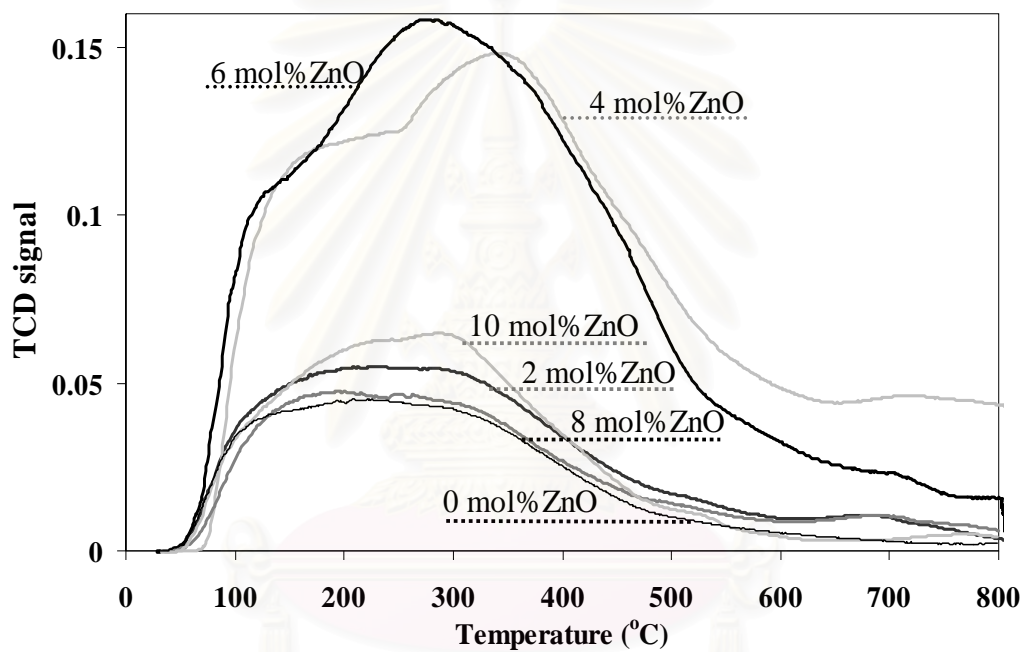


Figure 5.3 NH₃-TPD peaks of ZnO/TiO₂ films that contained various amount of ZnO.

สถาบันวิทยบริการ
จุฬาลงกรณ์มหาวิทยาลัย

Table 5.4 Surface acidity of ZnO/TiO₂ samples as determined from NH₃-TPD

Amount of ZnO (mol%)	Weight (g)	Strong acid peak area (mol H ⁺ /g)	Weak acid peak area (mol H ⁺ /g)	Total acid site (mol H ⁺ /g)
0	0.1048	0.2954	0.3372	0.6326
2	0.1046	0.4144	0.2468	0.6612
4	0.1106	1.3227	0.6610	1.9837
6	0.1088	1.4199	0.8225	2.2423
8	0.1052	0.4364	0.2154	0.6518
10	0.1042	0.6373	0.2673	0.9046

5.1.5 ESR results

Electron spin resonance (ESR) measurement was conducted using a JEOL JES-RE2X electron resonance spectrometer in order to determine the amount of Ti³⁺ on the surface of TiO₂ powder. The amount of Ti³⁺ was proportional to the intensity of ESR peak obtained. The spectrum of sample at room temperature mainly consisted of a split structure centered at a *g*-value close to 2. The results of ZnO/TiO₂ samples were displayed in Figure 5.4 and the peak areas together with the amount of Ti³⁺ on the surface of the samples were listed in Table 5.5. The amount of Ti³⁺ increased when ZnO was added. The maximum amounts of Ti³⁺ observed were for ZnO/TiO₂ with 4-6 mol% ZnO.

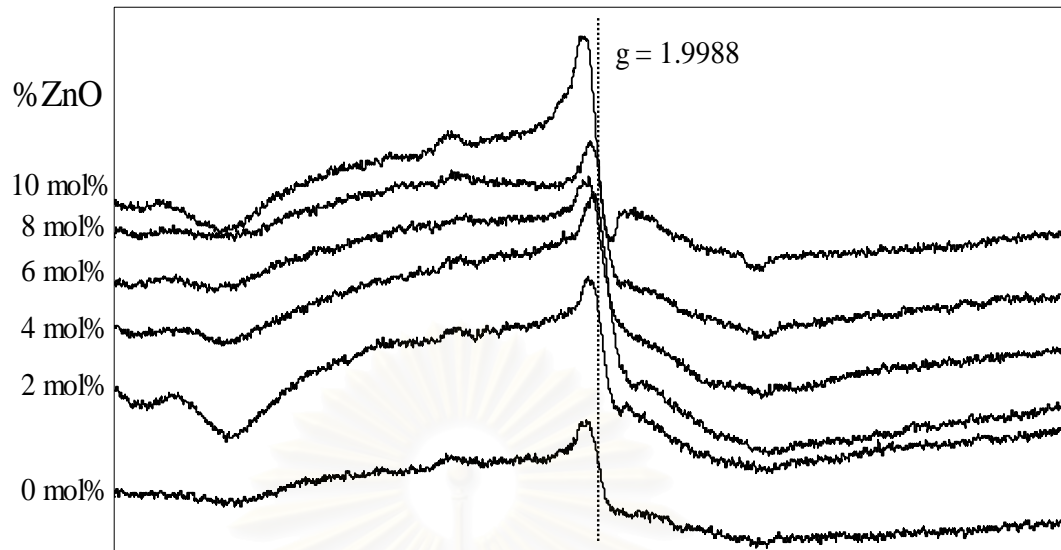


Figure 5.4 ESR results of ZnO/TiO₂ powders that contained various amount of ZnO

Table 5.5 Amount of Ti³⁺ surface defect in various ZnO/TiO₂ films as determined for ESR measurements.

Amount of ZnO (mol%)	Intensity of peak height	Weight (g)	Specific surface area (m ² g ⁻¹)	Intensity of Ti ³⁺ surface defects per area
0	1,277	0.3001	125.1	34.02
2	1,987	0.3104	123.8	51.71
4	2,629	0.3177	120.6	68.62
6	2,237	0.3047	101.2	72.55
8	1,988	0.3299	111.4	54.09
10	2,381	0.3250	123.8	59.18

5.1.6 Photo-induced hydrophilicity

Under UV irradiation, the contact angle of ZnO/TiO₂ thin film gradually decreased until the angle reached a steady value, called “saturated contact angle”. The results from contact angle measurements for ZnO/TiO₂ films that were calcined at 350 °C for two hours under stagnant air are presented in Figure 5.5. For pure TiO₂ film, the time needed to reach a saturated contact angle of ca. 5 degrees was approximately 120 minutes. When 4-6 mol% of ZnO was added to TiO₂ film, the time needed to reach a saturated contact angle shortened to approximately 40 minutes. However, when the amount of ZnO in ZnO/TiO₂ films exceeded 6 mol%, the time needed to reach a saturated contact angle grew longer and became close to the value for pure TiO₂ film at 10 mol% ZnO. Therefore, the optimal amount of ZnO in ZnO/TiO₂ film that gave rise to the highest hydrophilic property (or the shortest time to reach a saturated contact angle of ca. 5 degrees) was 4-6 mol% ZnO. These results appeared to be correlated with the amount of Ti³⁺ surface defect and the surface acidity of ZnO/TiO₂ films.

According to the results obtained for ESR measurements, the highest amount of Ti³⁺ surface defect was found in ZnO/TiO₂ films that contained 4-6 mol% ZnO (see Table 5.5). Ti³⁺ surface defect was an oxygen vacancy site, which brought about higher hydrophilic property of the surface [Giuseppe et al., 2000]

5.1.7 The sustainability of hydrophilicity of ZnO/TiO₂ film after removal of UV irradiation.

In order to assess the sustainability of hydrophilic property of ZnO/TiO₂ film, the films were placed in a dark box with no exposure to light as seen in Figure 5.6, the ZnO/TiO₂ thin films that was able to retain the hydrophilic properties for the longest time was the films that contained 4-6 mol% ZnO. The contact angle of those films remained below 10 degrees for 13 days while the contact angle of pure TiO₂ film grew beyond 10 degrees in merely 3 days. These observations suggested that the ZnO/TiO₂ films that were able to retain the hydrophilicity for the longest time appeared to be the films that possessed the highest hydrophilic properties (i.e., 4-6 mol% ZnO) to begin with.

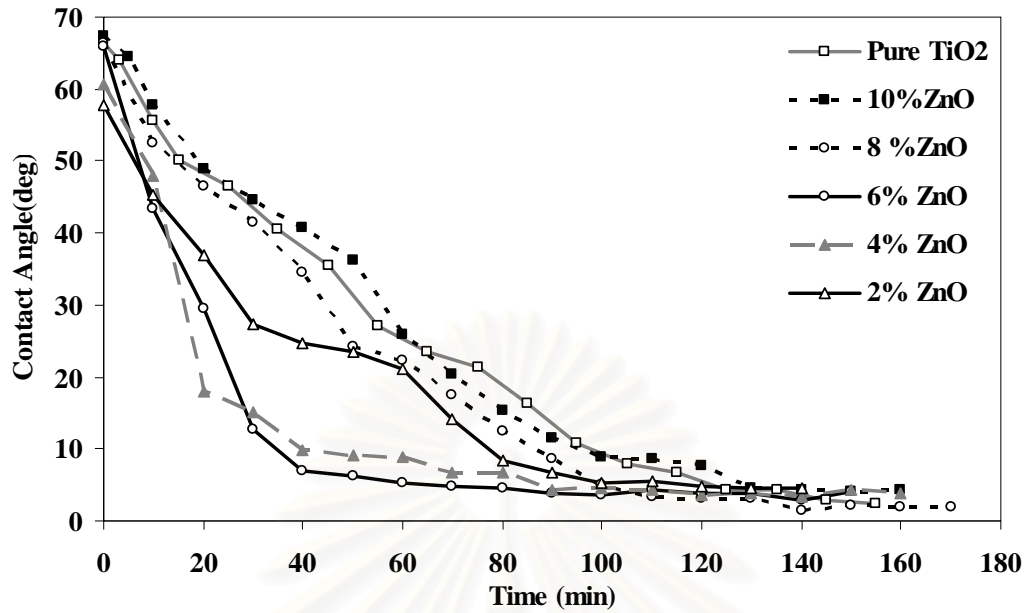


Figure 5.5 Change in contact angle of water droplet on the surfaces of various ZnO/TiO₂ films upon exposure to UV irradiation.

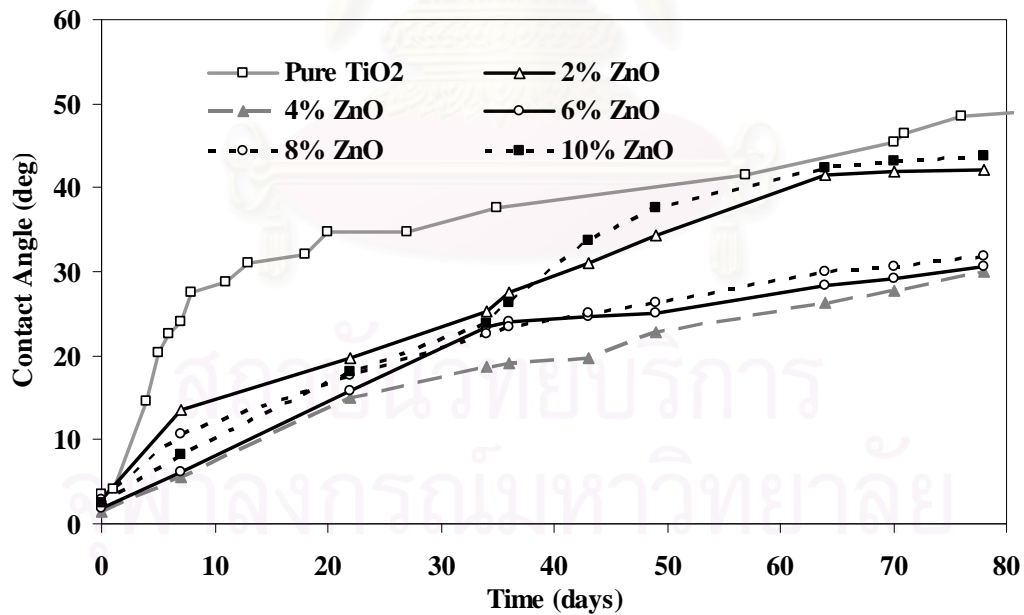


Figure 5.6 Change in contact angle of water droplet on the surface of various ZnO/TiO₂ films in the absence of UV irradiation.

5.2 Effect of addition of ZrO₂ to TiO₂ thin film.

5.2.1 Phase structures of ZrO₂/TiO₂

The bulk crystalline phases of samples were determined using X-ray diffractometer (XRD). ZrO₂/TiO₂ samples were prepared via a sol-gel method. The amount of ZrO₂ added was 2, 4, 6, 8, and 10 mol%. Then the films were calcined at 350 °C for two hours under atmospheres.

From the XRD patterns of ZrO₂/TiO₂ powder were calcined at 350 °C (see Figure 5.7), the dominant peak of anatase were observed at 2θ of about 25.2°, 37.9°, 47.8°, and 53.8°, which corresponded to the index of (101), (004), (200), and (105) plane, respectively. The weak peak at 2θ of 30.9° was assigned to brookite phase of TiO₂. XRD peaks that belong to rutile phase were not detected at this temperature. Even when the ZrO₂ content was as high as 10 mol%, none of XRD peaks associated with ZrO₂ were detected in any samples. Moreover, inspection of intensities of anatase peaks in the sample, which correlated with crystallinity of the sample, indicated that addition of ZrO₂ led to smaller diffraction peaks, thereby reducing the crystallinity of TiO₂. When amount of ZrO₂ was increased, the crystallinity of thin film was decreased further. The sample with 10 mol% of ZrO₂ possessed the lowest crystallinity when compared to the other samples.

Average crystallite size of anatase was determined from XRD pattern using the Scherrer equation. The results are listed in Table 5.6. Addition of ZrO₂ to TiO₂ appeared to increase the average crystallite size of anatase only slightly.

จุฬาลงกรณ์มหาวิทยาลัย

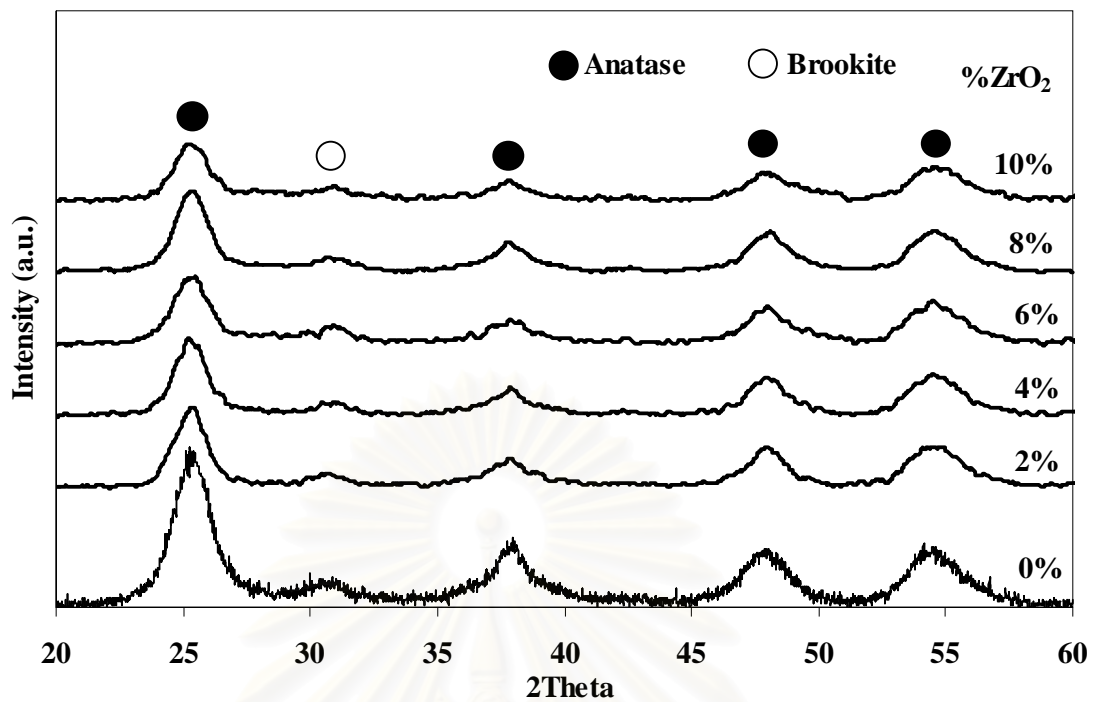


Figure 5.7 XRD patterns of $\text{ZrO}_2/\text{TiO}_2$ film calcined at $350\text{ }^\circ\text{C}$. The amount of ZrO_2 added was varied.

Table 5.6 Crystallite size of anatase in $\text{ZrO}_2/\text{TiO}_2$ with various amount of ZrO_2 , as determined from XRD patterns.

Amount of ZrO_2 (mol%)	Crystallite size (nm)
0	4.5
2	5.4
4	5.5
6	4.9
8	5.2
10	5.5

5.2.2 Surface morphology of ZrO₂/TiO₂ thin film

Figure 5.8 shows the surface topography images of ZrO₂/TiO₂ thin films coated on glass surfaces. The surface images of ZrO₂/TiO₂ thin films with 0%, 2%, 4%, 6%, 8%, and 10% mol ZrO₂ are shown in Figure 5.8 (a), (b), (c), (d), (e), and (f), respectively.

Analysis of AFM images suggests that addition of ZrO₂ into TiO₂ increased the grain size of TiO₂. The more ZrO₂ added, the larger the grain size (see Table 5.7). However, the average roughness of the ZrO₂/TiO₂ film surface appeared not to be effected by the addition of ZrO₂.

Table 5.7 Grain size and average roughness of ZrO₂/TiO₂ thin film as determined from AFM images

Amount of ZrO ₂ (mol%)	Grain size (nm)	Average Roughness From AFM (nm)
0	2.468	2.631
2	2.613	2.272
4	1.620	2.865
6	1.849	2.556
8	2.151	2.909
10	1.742	2.675

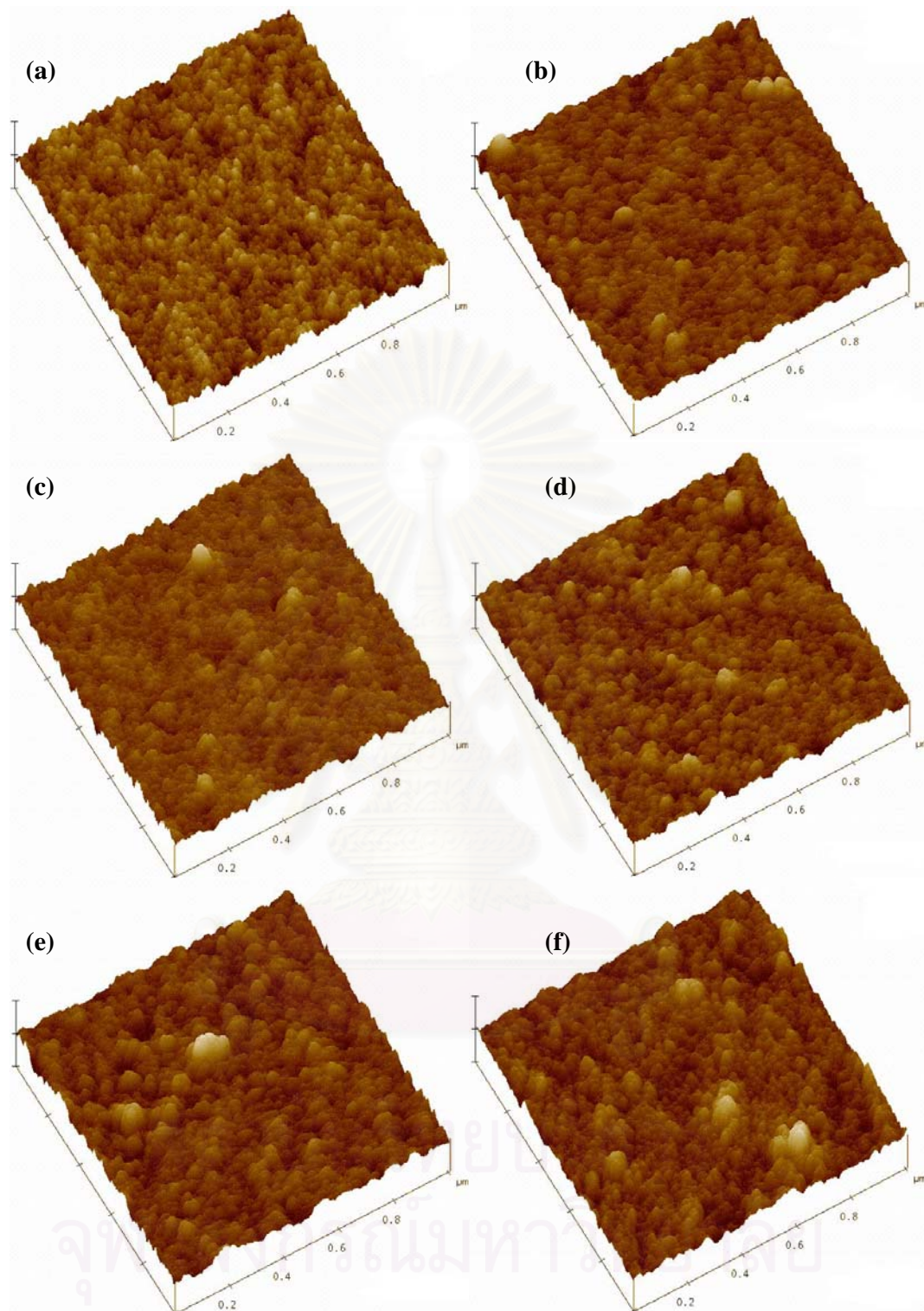


Figure 5.8 AFM images of ZrO₂/TiO₂ film surface that contained a) 0%, b) 2%, c) 4%, d) 6%, e) 8%, and f) 10% mol of ZrO₂.

5.2.3 Specific surface area of ZrO₂/TiO₂

The most common procedure for determining surface area of a solid is based on adsorption and condensation of nitrogen at liquid nitrogen temperature using static vacuum procedure. This method is also called BET (Brunauer Emmett Teller) method using nitrogen as the adsorption at 77 K in a Micromeritics Chemisorb 2750 automated system. Specific surface area of ZrO₂/TiO₂ was measured. The samples were dried at 200 °C for one hour in a 30% N₂/He flow prior to BET measurements. The measured BET surface areas of titanium dioxide samples were in the range of 104.6-142.0 m²/g (see Table 5.8). The addition of ZrO₂ did not have a significant effect on the specific surface area of the mixed oxide.

Table 5.8 Specific surface area of ZrO₂/TiO₂ with various amount of ZrO₂.

Amount of ZrO ₂ (mol%)	Specific surface area (m ² /g)
0	125.1
2	104.6
4	125.3
6	142.0
8	122.2
10	123.3

สถาบันวิทยบริการ
จุฬาลงกรณ์มหาวิทยาลัย

5.2.4 Temperature Programmed Desorption (TPD)

Temperature-programmed desorption using ammonia as a probe molecule was employed to determine the amount of the acid site on $\text{ZrO}_2/\text{TiO}_2$ powders. The results are shown in Table 5.9. The overall surface acidity of $\text{ZrO}_2/\text{TiO}_2$ Film increased as the content of ZrO_2 in the film increased. These results were in good agreement with the results from Laniecki and coworker [2006]. The highest amount of surface acidity was observed in $\text{ZrO}_2/\text{TiO}_2$ film that contained 10 mol% ZrO_2 (see Figure 5.9).

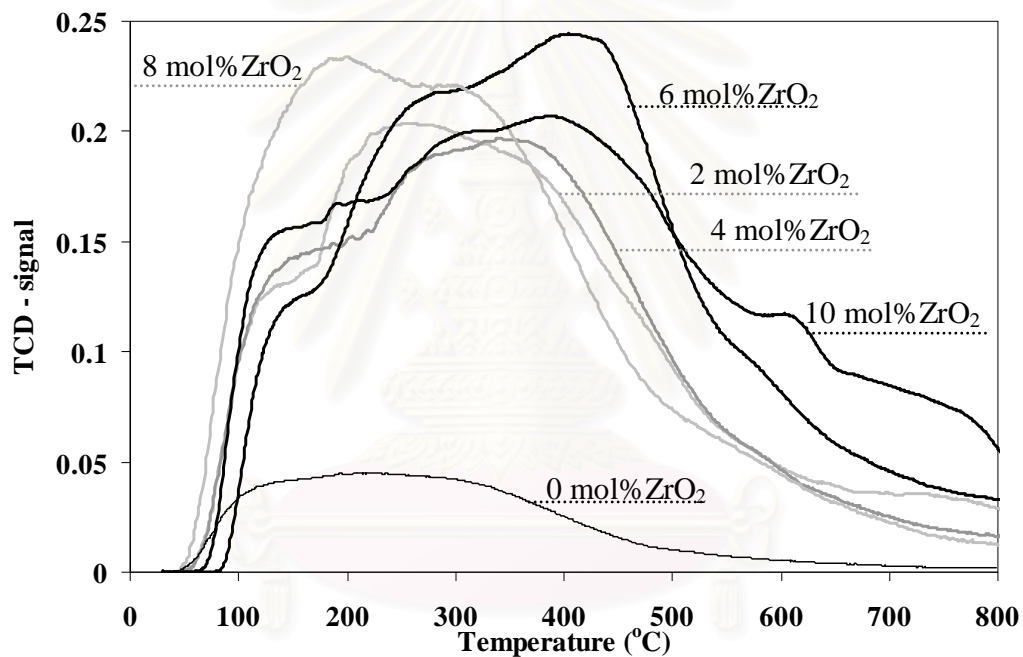


Figure 5.9 NH_3 -TPD peaks of $\text{ZrO}_2/\text{TiO}_2$ films that contained various amount of ZrO_2 .

Table 5.9 Surface of acidity of ZrO₂/TiO₂ samples as determined from NH₃-TPD

Amount of ZrO ₂ (mol%)	Weight (g)	Strong acid peak area (mol H ⁺ /g)	Weak acid peak area (mol H ⁺ /g)	Total acid site (mol H ⁺ /g)
0	0.1048	0.2954	0.3372	0.6326
2	0.1065	1.9111	0.8305	2.7416
4	0.1054	1.6544	1.0627	2.7171
6	0.1096	2.0066	0.7184	2.7249
8	0.1074	0.7641	1.0841	1.8482
10	0.1054	1.6165	1.2325	2.8490

5.2.5 ESR results

Electron spin resonance (ESR) measurement was conducted using a JEOL JES-RE2X electron resonance spectrometer in order to determine the amount of Ti³⁺ on the surface of TiO₂ powder. The amount of Ti³⁺ was proportional to the intensity of ESR peak obtained. The spectrum of sample at room temperature mainly consisted of a split structure centered at a *g*-value close to 2. The results of ZrO₂/TiO₂ samples were displayed in Figure 5.10 and the peak areas together with the amount of Ti³⁺ on the surface of the samples were listed in Table 5.10. The amount of Ti³⁺ increased when ZrO₂ was added. The maximum amounts of Ti³⁺ observed were for ZrO₂/TiO₂ with 10 mol% ZrO₂.

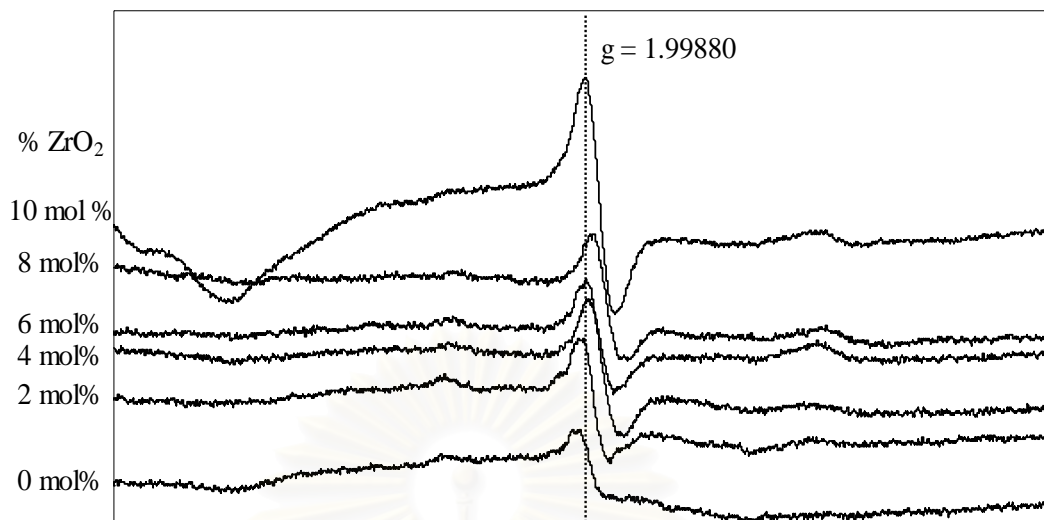


Figure 5.10 ESR results of $\text{ZrO}_2/\text{TiO}_2$ powders that contained various amount of ZrO_2

Table 5.10 Amount of Ti^{3+} surface defect in various $\text{ZrO}_2/\text{TiO}_2$ films as determined for ESR measurements

Amount of ZrO_2 (mol%)	Intensity of peak height	Weight (g)	Specific surface area ($\text{m}^2 \text{g}^{-1}$)	Intensity of Ti^{3+} surface defects per area
0	1,277	0.3001	125.1	34.02
2	1,696	0.3161	104.6	51.29
4	1,886	0.3061	125.3	49.17
6	1,553	0.3045	142.0	35.92
8	1,714	0.3163	122.2	44.34
10	3,215	0.3155	123.3	82.65

5.2.6 Photo-induced hydrophilicity

Under UV irradiation, the contact angle of $\text{ZrO}_2/\text{TiO}_2$ thin film gradually decreased until the angle reached a steady value, called “saturated contact angle”. The results from contact angle measurements for $\text{ZrO}_2/\text{TiO}_2$ films that were calcined at $350\text{ }^\circ\text{C}$ for two hours under stagnant air are presented in Figure 5.11. For pure TiO_2 film, the time needed to reach a saturated contact angle of ca. 5 degrees was approximately 120 minutes. When 10 mol% of ZrO_2 was added to TiO_2 film, the time needed to reach a saturated contact angle shortened to approximately 40 minutes. When the amount of ZrO_2 in $\text{ZrO}_2/\text{TiO}_2$ films exceeded to 10 mol%, the time needed to reach a saturated contact angle grew longest. Therefore, the optimal amount of ZrO_2 in $\text{ZrO}_2/\text{TiO}_2$ film that gave rise to the highest hydrophilic property (or the shortest time to reach a saturated contact angle of ca. 5 degrees) was 10 mol% ZrO_2 . These results appeared to be correlated with the amount of Ti^{3+} surface defect and the surface acidity of $\text{ZrO}_2/\text{TiO}_2$ films.

According to the results obtained for ESR measurements, the highest amount of Ti^{3+} surface defect was found in $\text{ZrO}_2/\text{TiO}_2$ films that contained 10 mol% ZrO_2 (see Table 5.10). Ti^{3+} surface defect was an oxygen vacancy site, which brought about higher hydrophilic property of the surface

5.2.7 The sustainability of hydrophilicity of $\text{ZrO}_2/\text{TiO}_2$ film after removal of UV irradiation.

In order to assess the sustainability of hydrophilic property of $\text{ZrO}_2/\text{TiO}_2$ film, the films were placed in a dark box with no exposure to light as seen in Figure 5.12, the $\text{ZrO}_2/\text{TiO}_2$ thin films that was able to retain the hydrophilic properties for the longest time was the films that contained 10 mol% ZrO_2 . The contact angle of those films remained below 10 degrees for 13 days while the contact angle of pure TiO_2 film grew beyond 10 degrees in merely 3 days. These observations suggested that the $\text{ZrO}_2/\text{TiO}_2$ films that were able to retain the hydrophilicity for the longest time appeared to be the films that possessed the highest hydrophilic properties (i.e., 10 mol% ZrO_2) to begin with.

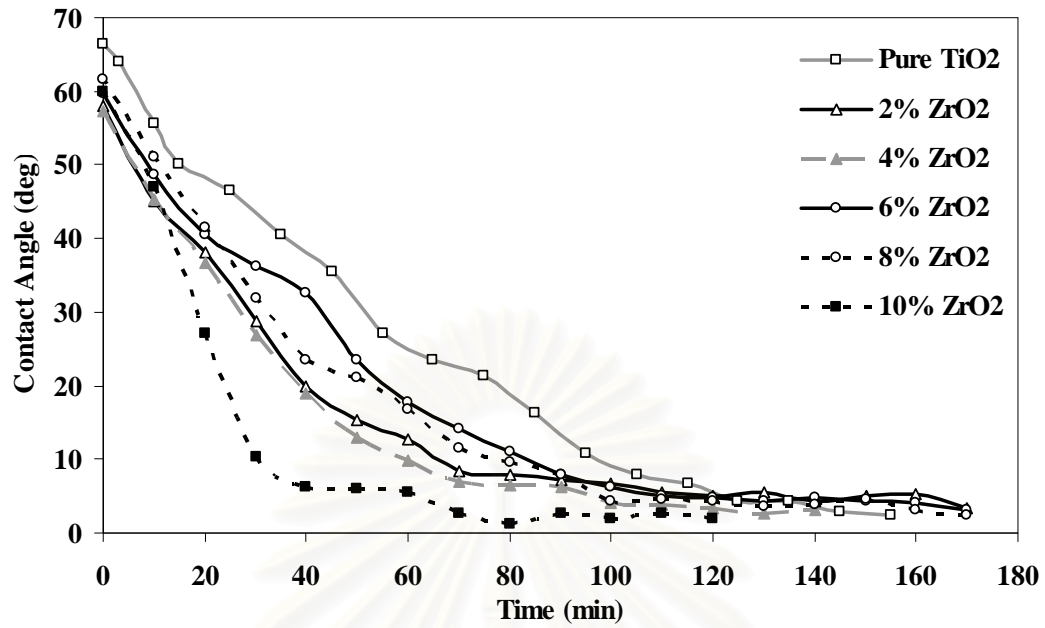


Figure 5.11 Change in contact angle of water droplet on the surfaces of various ZrO_2/TiO_2 films upon exposure to UV irradiation.

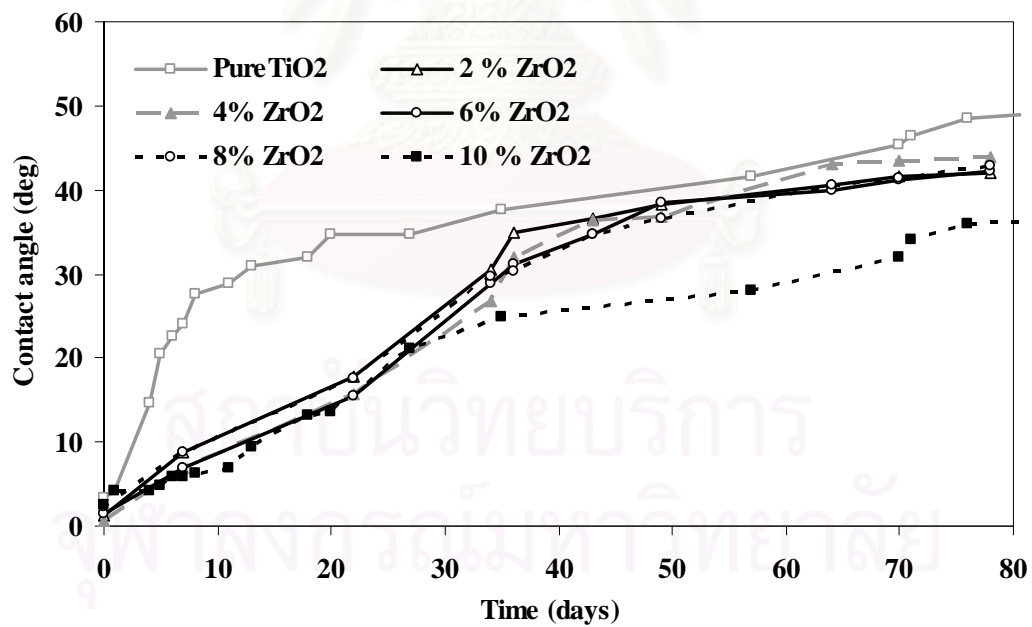


Figure 5.12 Change in contact angle of water droplet on the surface of various ZrO_2/TiO_2 films in the absence of UV irradiation

5.3 Effect of addition of Fe₂O₃ to TiO₂

5.3.1 Phase structures of Fe₂O₃/TiO₂

The bulk crystalline phases of samples were determined using X-ray diffractometer (XRD). Fe₂O₃/TiO₂ samples were prepared via a sol-gel method. The amount of Fe₂O₃ added was 2, 4, 6, 8, and 10 mol%. Then the films were calcined at 350 °C for two hours under atmospheres.

From the XRD patterns of Fe₂O₃/TiO₂ powder were calcined at 350 °C (see Figure 5.13), the dominant peak of anatase were observed at 2θ of about 25.2°, 37.9°, 47.8°, and 53.8°, which corresponded to the index of (101), (004), (200), and (105) plane, respectively. The weak peak at 2θ of 30.9° was assigned to brookite phase of TiO₂. XRD peaks that belong to rutile phase were not detected at this temperature. Even when the content of the Fe₂O₃ was as high as 10 mol%, none of crystalline phases of rutile was detected in any samples. Moreover, inspection of intensities of anatase peaks in the sample, which correlated with crystallinity of the sample, revealed that the addition of Fe₂O₃ led to larger diffraction peaks than pure titania sample that is an increase in the crystallinity of anatase in Fe₂O₃/TiO₂. Nevertheless, an increase in the amount of Fe₂O₃ from 2 to 10 mol% did not have an effect on the crystallinity of anatase, which was evident from similar XRD peak intensities observed for the various loading of Fe₂O₃.

Average crystallite size of anatase was determined from XRD pattern using the Scherrer equation. The results are listed in Table 5.11. Addition of Fe₂O₃ to TiO₂ appeared to increase the average crystallite size of anatase only slightly.

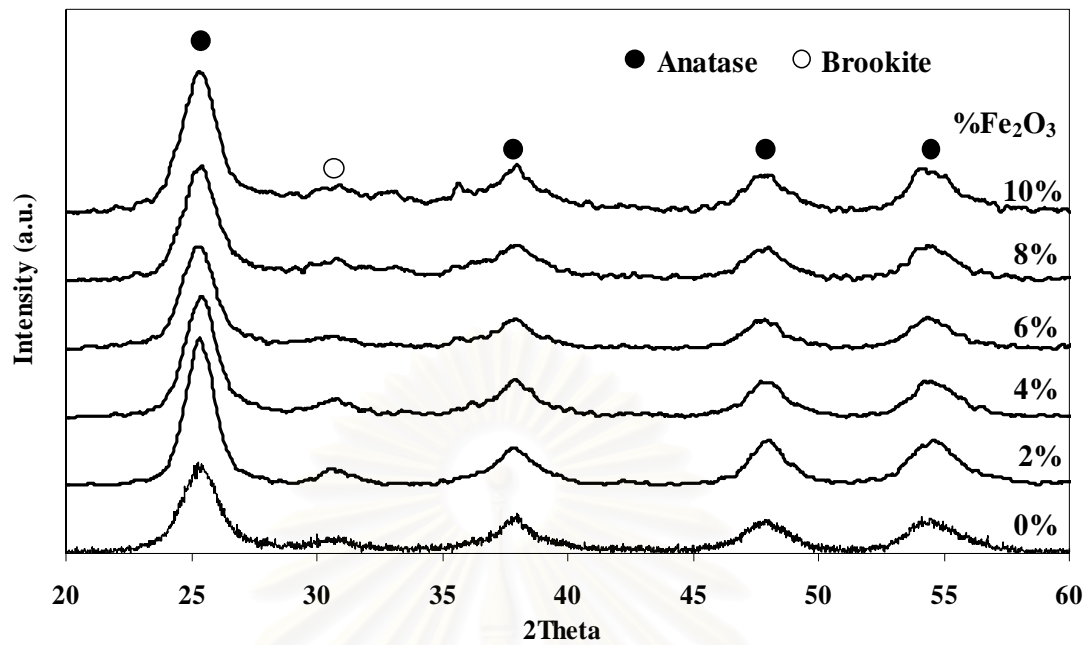


Figure 5.13 XRD patterns of $\text{Fe}_2\text{O}_3/\text{TiO}_2$ film calcined at 350°C . The amount of Fe_2O_3 was varied added.

Table 5.11 Crystallite size of anatase in $\text{Fe}_2\text{O}_3/\text{TiO}_2$ with various amount of Fe_2O_3 , as determined from XRD pattern.

Amount of Fe_2O_3 (mol%)	Crystallite size (nm)
0	4.5
2	6.0
4	5.5
6	5.1
8	5.0
10	4.8

5.3.2 Surface morphology of Fe₂O₃/TiO₂ thin film

Figure 5.14 shows the surface topography images of Fe₂O₃/TiO₂ thin film coated on glass surfaces. The surface images of Fe₂O₃/TiO₂ thin film with 0%, 2%, 4%, 6%, 8%, and 10% mol Fe₂O₃ are shown in Figures 5.14 (a), (b), (c), (d), (e), and (f), respectively.

Analysis of AFM images suggests that addition of Fe₂O₃ into TiO₂ increased the grain size of TiO₂. The more Fe₂O₃ added, the larger the grain size (see Table 5.12). However, the average roughness of the Fe₂O₃/TiO₂ film surface appeared not to be effected by the addition of Fe₂O₃.

Table 5.12 Grain size and average roughness of Fe₂O₃/TiO₂ thin film as determined from AFM images

Amount of Fe ₂ O ₃ (mol%)	Grain size (nm)	Average Roughness From AFM (nm)
0	2.468	2.631
2	2.950	2.874
4	1.930	2.336
6	2.409	2.273
8	2.476	2.306
10	1.477	2.436

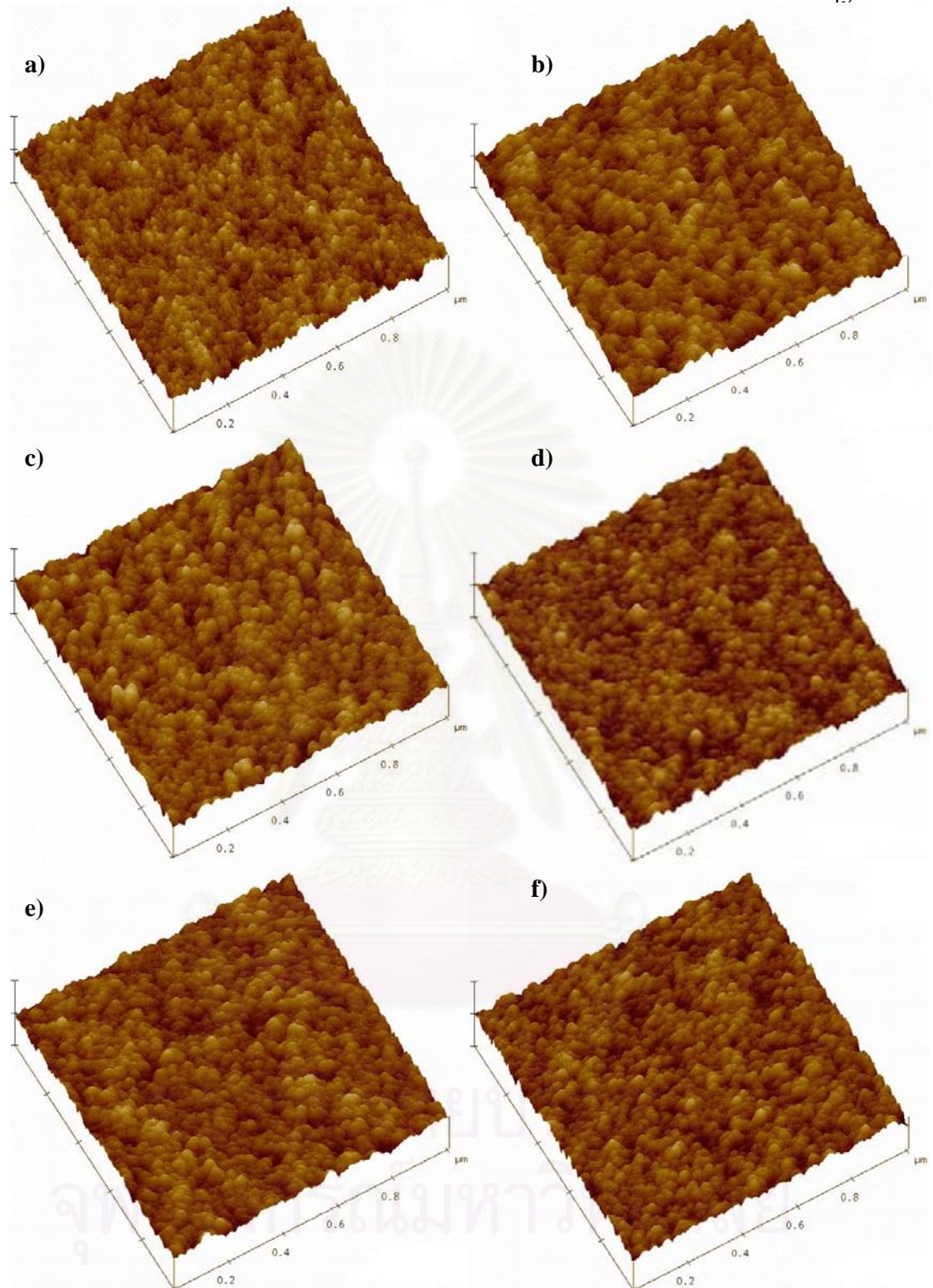


Figure 5.14 AFM images of Fe₂O₃/TiO₂ film surfaces that contained a) 0%, b) 2%, c) 4%, d) 6%, e) 8%, and f) 10% mol of Fe₂O₃.

5.3.3 Specific surface area of Fe₂O₃/TiO₂

The most common procedure for determining surface area of a solid is based on adsorption and condensation of nitrogen at liquid nitrogen temperature using static vacuum procedure. This method is also call BET (Brunauer Emmett Teller) method using nitrogen as the adsorption at 77 K in a Micromeritics Chemisorb 2750 automated system. Specific surface area of Fe₂O₃/TiO₂ was measured. The samples were dried at 200 °C for 1 hour in a 30% N₂/He flow prior to BET measurements. The measured BET surface areas of titanium dioxide samples were in the range of 100.7-125.1 m²/g (see Table 5.13). The addition of Fe₂O₃ did not have a significant effect on the specific surface area of the mixed oxide.

Table 5.13 Specific surface area of Fe₂O₃/TiO₂ with various amount of Fe₂O₃.

Amount of Fe ₂ O ₃ (mol%)	BET Surface Area (m ² /g)
0	125.1
2	117.5
4	100.7
6	110.9
8	123.7
10	105.4

สถาบันวิทยบริการ
จุฬาลงกรณ์มหาวิทยาลัย

5.3.4 Temperature Programmed Desorption (TPD)

Temperature-programmed desorption using ammonia as a probe molecule was employed to determine the amount of the acid site on $\text{Fe}_2\text{O}_3/\text{TiO}_2$ powders. The results are shown in Table 5.14. Addition of Fe_2O_3 to TiO_2 reduced the total number of acid sites slightly – i.e., the surface acidity of $\text{Fe}_2\text{O}_3/\text{TiO}_2$ was slightly lower than that of pure TiO_2 (see Figure 5.15).

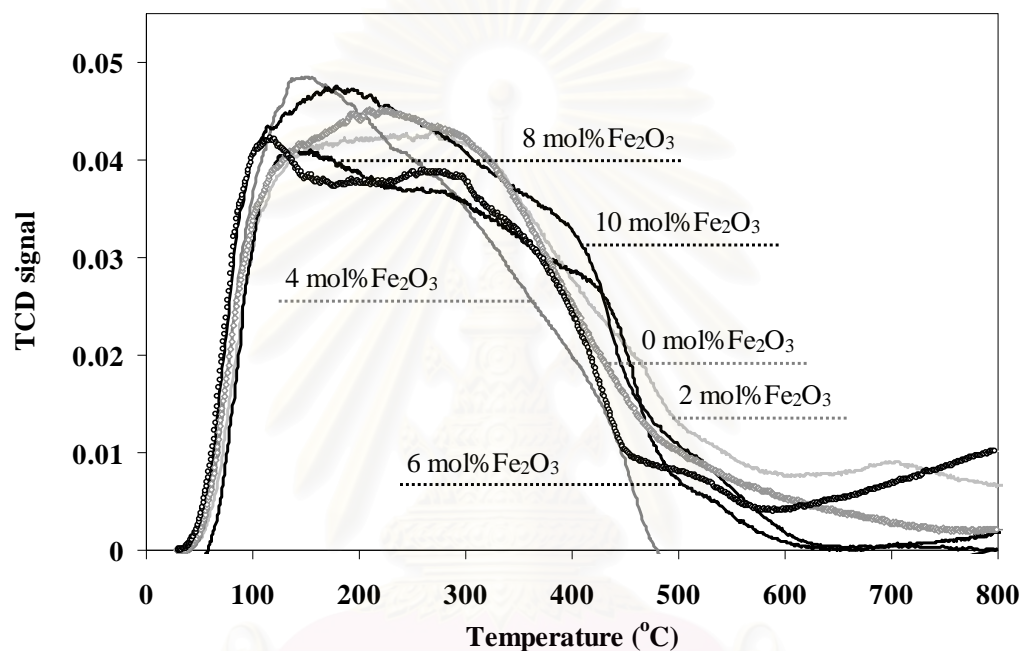


Figure 5.15 NH_3 -TPD peaks of $\text{Fe}_2\text{O}_3/\text{TiO}_2$ films that contained various amount of Fe_2O_3 .

Table 5.14 Surface acidity of $\text{Fe}_2\text{O}_3/\text{TiO}_2$ samples as determined from NH_3 -TPD

Amount of Fe_2O_3 (mol%)	Weight (g)	Strong acid peak area (mol H^+ /g)	Weak acid peak area (mol H^+ /g)	Total acid site (mol H^+ /g)
0	0.1048	0.2954	0.3372	0.6326
2	0.1028	0.2829	0.3299	0.6128
4	0.1032	0.2166	0.4619	0.6785
6	0.1044	0.1733	0.4838	0.6571
8	0.1045	0.1741	0.3689	0.5429
10	0.1054	0.2059	0.5228	0.7287

5.3.5 ESR results

Electron spin resonance (ESR) measurement was conducted using a JEOL JES-RE2X electron resonance spectrometer in order to determine the amount of Ti^{3+} on the surface of TiO_2 powder. The spectrum of sample at room temperature mainly consisted of a split structure centered at a g -value close to 2. However, the peak corresponding to Ti^{3+} was not detected due to an interference of Ti^{3+} peak from Fe^{3+} peak, which was in close proximity with each other. The g -value of Fe^{3+} and Ti^{3+} (anatase phase) were about 2.435 and 0.1991, respectively. (see Figure 5.16).

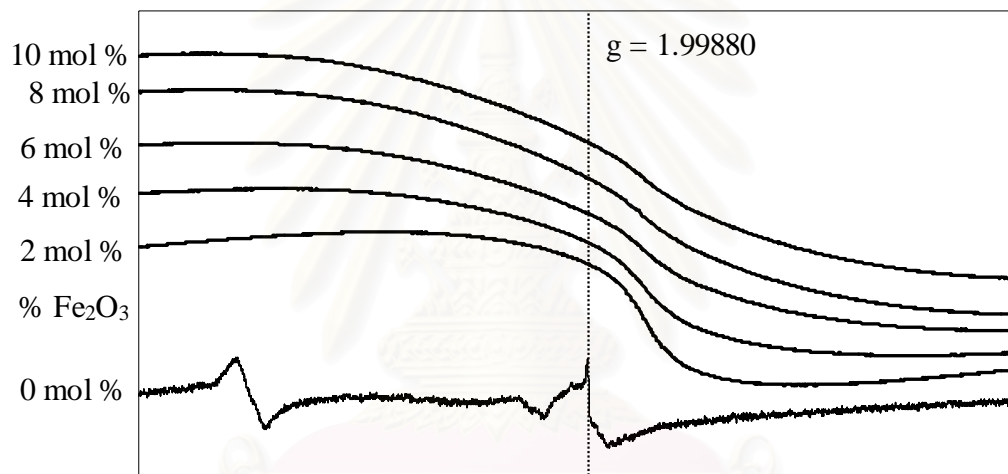


Figure 5.16 ESR results of $\text{Fe}_2\text{O}_3/\text{TiO}_2$ powders that contained various amount of Fe_2O_3 .

สถาบันวิทยบริการ
จุฬาลงกรณ์มหาวิทยาลัย

5.3.6 Photo-induced hydrophilicity

The results from contact angle measurements for $\text{Fe}_2\text{O}_3/\text{TiO}_2$ films that were calcined at $350\text{ }^\circ\text{C}$ for two hours under stagnant air are presented in Figure 5.17. For pure TiO_2 film, the time needed to reach a saturated contact angle of ca. 5 degrees was approximately 120 minutes. However, when Fe_2O_3 was added to TiO_2 , the time needed to reach a saturated contact angle increased to 150 minutes for all $\text{Fe}_2\text{O}_3/\text{TiO}_2$ films. So $\text{Fe}_2\text{O}_3/\text{TiO}_2$ film possessed worse hydrophilic properties than TiO_2 film did. These findings were in good agreement with the result from NH_3 -TPD, which found the surface acidity of $\text{Fe}_2\text{O}_3/\text{TiO}_2$ to be lower than that of pure TiO_2 .

5.3.7 The sustainability of hydrophilicity of thin film after removal of UV irradiation.

As seen in Figure 5.18, the ability to retain the hydrophilic property of $\text{Fe}_2\text{O}_3/\text{TiO}_2$ films after removal of UV irradiation was worse than that of pure TiO_2 film. These findings agreed with observation previously mentioned that the film with better hydrophilic property could retain the hydrophilic property longer.

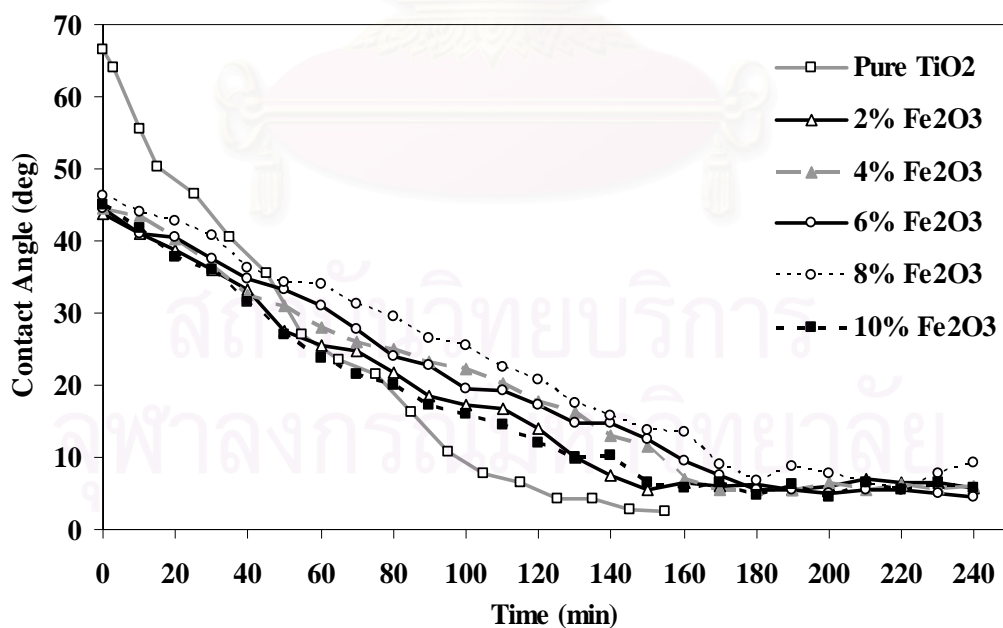


Figure 5.17 Change in contact angle of water droplet on the surfaces of various $\text{Fe}_2\text{O}_3/\text{TiO}_2$ films upon exposure to UV irradiation.

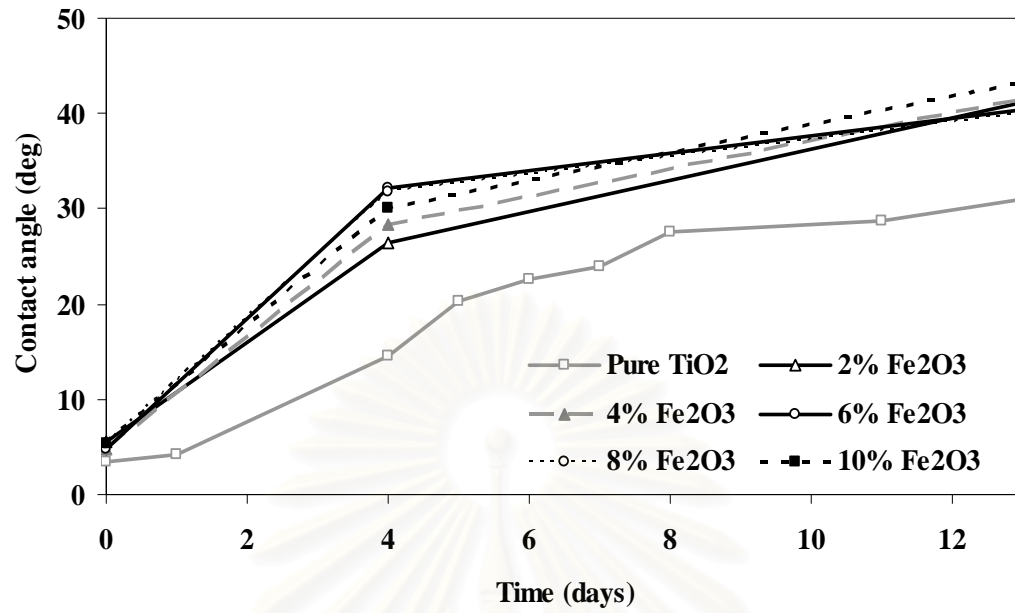


Figure 5.18 Change in contact angle of water droplet on the surface various Fe₂O₃/TiO₂ films in the absence of UV irradiation.

สถาบันวิทยบริการ
จุฬาลงกรณ์มหาวิทยาลัย

CHAPTER VI

CONCLUSIONS AND RECOMMENDATION

6.1 Conclusions

The conclusions of this research are as follows:

1. ZnO and ZrO₂ can be added to TiO₂ to improve hydrophilic property of the mixed oxide films. The amount of the second metal oxide that produced mixed oxide film with the best hydrophilicity are 4-6 mol% for ZnO and 10 mol% for ZrO₂.
2. Fe₂O₃/TiO₂ films that contained 2-10 mol% Fe₂O₃ possess worse hydrophilicity than that of pure TiO₂ film.
3. There seems to be a correlation between hydrophilic property of thin film and both the amount of Ti³⁺ surface defect and the acidity of the surface.
4. The better the hydrophilic property of the film, the long the ability of the film to retain its hydrophilicity after removal UV irradiation.

6.2 Recommendation for future studies

The following recommendations for future studies are proposed.

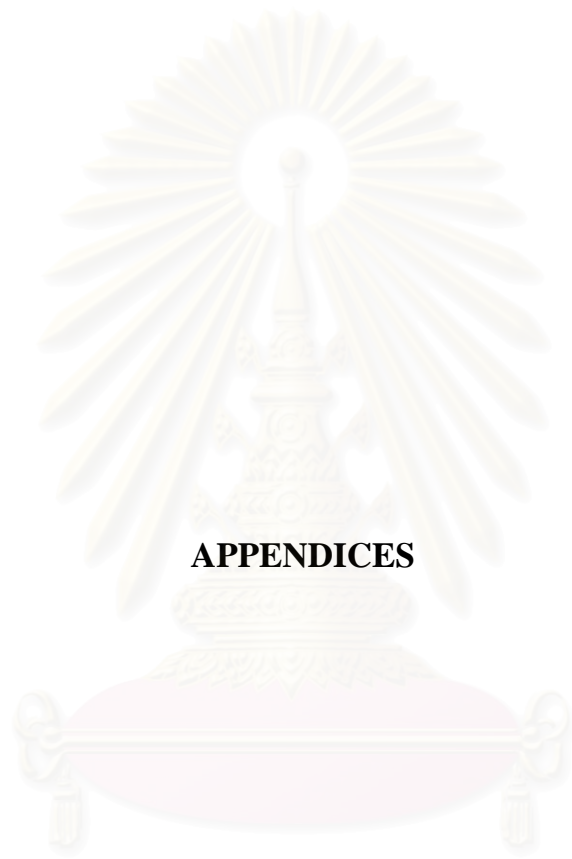
1. Other preparation for prepare TiO₂ thin film should be tried.
2. Other element for addition to TiO₂ thin film should be tried.
3. The film sample was used in another application such as decomposition the hydrocarbon compound, treat the water and air pollution.

REFERENCES

- Celik, E., Yildiz, A. Y., Ak Azem, N. F., Tanoglu, M., Toparli, M., Emrullahoglu, O. F., and Ozdemir, I. (2006). "Preparation and characterization of Fe₂O₃-TiO₂ thin films on glass substrate for photocatalytic applications." *Materials Science and Engineering: B*, 129(1-3), 193-199.
- De Gennes, P. G. (1985). "Wetting: Statics and dynamics " *Reviews of Modern Physics* 57(3), 827-863.
- Fu, X., Clark, L. A., Zeltner, W. A., and Anderson, M. A. (1996). "Effects of reaction temperature and water vapor content on the heterogeneous photocatalytic oxidation of ethylene." *Journal of Photochemistry and Photobiology A: Chemistry*, 97(3), 181-186.
- Fujishima, A., Hashimoto, K., and Watanabe, T. (1999). *TiO₂ photocatalysis: fundamental and applications. 1st ed*, BKC, Tokyo.
- Fujishima, A., Rao, T. N., and Tryk, D. A. (2000). "Titanium dioxide photocatalysis." *Journal of Photochemistry and Photobiology C: Photochemistry Reviews*, 1(1), 1-21.
- Guan, K. (2005). "Relationship between photocatalytic activity, hydrophilicity and self-cleaning effect of TiO₂/SiO₂ films." *Surface and Coatings Technology*, 191(2-3), 155-160.
- Hernandez-Alonso, M. D., Tejedor-Tejedor, I., Coronado, J. M., Soria, J., and Anderson, M. A. (2006). "Sol-gel preparation of TiO₂-ZrO₂ thin films supported on glass rings: Influence of phase composition on photocatalytic activity." *Thin Solid Films*, 502(1-2), 125-131.

- Kang, M., Choung, S.-J., and Park, J. Y. (2003). "Photocatalytic performance of nanometer-sized $\text{Fe}_x\text{O}_y/\text{TiO}_2$ particle synthesized by hydrothermal method." *Catalysis Today*, 87(1-4), 87-97.
- Lee, Y. C., Hong, Y. P., Lee, H. Y., Kim, H., Jung, Y. J., Ko, K. H., Jung, H. S., and Hong, K. S. (2003). "Photocatalysis and hydrophilicity of doped TiO_2 thin films." *Journal of Colloid and Interface Science*, 267(1), 127-131.
- Łencka, M. M., and Riman, R.E. (1993). "Thermodynamic modeling of hydrothermal synthesis of ceramic powders " *Chemistry of Materials* 5(1), 61-70.
- Liao, S., Donggen, H., Yu, D., Su, Y., and Yuan, G. (2004). "Preparation and characterization of ZnO/TiO_2 , $\text{SO}_4^{2-}/\text{ZnO}/\text{TiO}_2$ photocatalyst and their photocatalysis." *Journal of Photochemistry and Photobiology A: Chemistry*, 168(1-2), 7-13.
- Linsebigler, A. L., Lu, G., and Yates Jr., J.T. (1995). "Photocatalysis on TiO_2 surfaces: Principles, mechanisms, and selected results " *Chemical Reviews* 95(3), 735-758.
- Litter, M. I. (1999). "Heterogeneous photocatalysis: Transition metal ions in photocatalytic systems." *Applied Catalysis B: Environmental*, 23(2-3), 89-114.
- Maeda, M., and Hirota, K. (2006). "Characterization of titanium-tin composite oxide films and their visible-light photocatalytic properties." *Applied Catalysis A: General*, 302(2), 305-308.
- Marci, G., Loddo, V., Martin, C., Palmisano, L., Rives, V., and Sclafani, A. (1999). "Preparation and characterisation of TiO_2 (anatase) supported on TiO_2 (rutile) catalysts employed for 4-nitrophenol photodegradation in aqueous medium and comparison with TiO_2 (anatase) supported on Al_2O_3 ." *Applied Catalysis B: Environmental*, 20(1), 29-45.

- Othmer, K. (1991). *Encyclopedia of chemical technology*, J. Wiley&Son, translator, Wiley-Interscience Publication, New York.
- Su, C., Hong, B. Y., and Tseng, C. M. (2004). "Sol-gel preparation and photocatalysis of titanium dioxide." *Catalysis Today*, 96(3), 119-126.
- Sun, R.-D., Nakajima, A., Fujishima, A., Watanabe, T., and Hashimoto, K. (2001). "Photoinduced surface wettability conversion of ZnO and TiO₂ Thin Films" *Journal of Physical Chemistry B*, 105(10), 1984-1990.
- Watanabe, T., Nakajima, A., Wang, R., Minabe, M., Koizumi, S., Fujishima, A., and Hashimoto, K. (1999). "Photocatalytic activity and photoinduced hydrophilicity of titanium dioxide coated glass." *Thin Solid Films*, 351(1-2), 260-263.
- Xin, B., Ren, Z., Wang, P., Liu, J., Jing, L., and Fu, H. (2007). "Study on the mechanisms of photoinduced carriers separation and recombination for Fe³⁺-TiO₂ photocatalysts." *Applied Surface Science*, 253(9), 4390-4395.
- Yu, J., and Zhao, X. (2001a). "Effect of surface treatment on the photocatalytic activity and hydrophilic property of the sol-gel derived TiO₂ thin films." *Materials Research Bulletin* 36(1-2), 97-107.
- Yu, J., and Zhao, X. . (2001b). "Effect of surface microstructure on the super-hydrophilic property of the sol-gel derived porous TiO₂ thin films." *Journal of Materials Science Letters*, 20(7), 671-673
- Yu, J. C., Yu, J., Ho, W., and Zhao, J. (2002). "Light-induced super-hydrophilicity and photocatalytic activity of mesoporous TiO₂ thin films." *Journal of Photochemistry and Photobiology A: Chemistry*, 148(1-3), 331-339.



APPENDICES

สถาบันวิทยบริการ
จุฬาลงกรณ์มหาวิทยาลัย

APPENDIX A

CALCULATION OF THE CRYSTALLITE SIZE

Calculation of the crystallite size by Debye-Scherrer equation

The crystallite size is calculated from the width at half-height of the diffraction peak of XRD pattern using the Debye-Scherrer equation.

From Scherrer equation:

$$D = \frac{K\lambda}{\beta \cos \theta} \quad (\text{A.1})$$

- where
- D = crystallite size, Å
 - K = crystallite-shape factor = 0.9
 - λ = X-ray wavelength, 1.5418 Å for CuK α
 - θ = observed peak angle, degree
 - β = X-ray diffraction broadening, radian

The X-ray diffraction broadening (β) is the pure width of a powder diffraction, free of all broadening due to the experimental equipment. Standard α -alumina is used to observe the instrumental broadening since its crystallite size is larger than 2000 Å. The X-ray diffraction broadening (β) can be obtained by using Warren's formula.

From Warren's formula:

$$\begin{aligned} \beta^2 &= B_M^2 - B_S^2 \\ \beta &= \sqrt{B_M^2 - B_S^2} \end{aligned} \quad (\text{A.2})$$

- Where
- B_M = the measured peak width in radians at half peak height.
 - B_S = the corresponding width of a standard material.

Example: Calculation of the crystallite size of titania

$$\begin{aligned} \text{The half-height width of 101 diffraction peak} &= 1.80813^\circ \\ &= 0.03156 \text{ radian} \end{aligned}$$

$$\text{The corresponding half-height width of peak of titania} = 0.004 \text{ radian}$$

$$\begin{aligned} \text{The pure width} &= \sqrt{B_M^2 - B_S^2} \\ &= \sqrt{0.03156^2 - 0.004^2} \\ &= 0.03132 \text{ radian} \end{aligned}$$

$$\beta = 0.03132 \text{ radian}$$

$$2\theta = 25.28^\circ$$

$$\theta = 12.64^\circ$$

$$\lambda = 1.5418 \text{ \AA}$$

$$\begin{aligned} \text{The crystallite size} &= \frac{0.9 \times 1.5418}{0.03132 \cos 12.64} = 45.40 \text{ \AA} \\ &= 4.5 \text{ nm} \end{aligned}$$

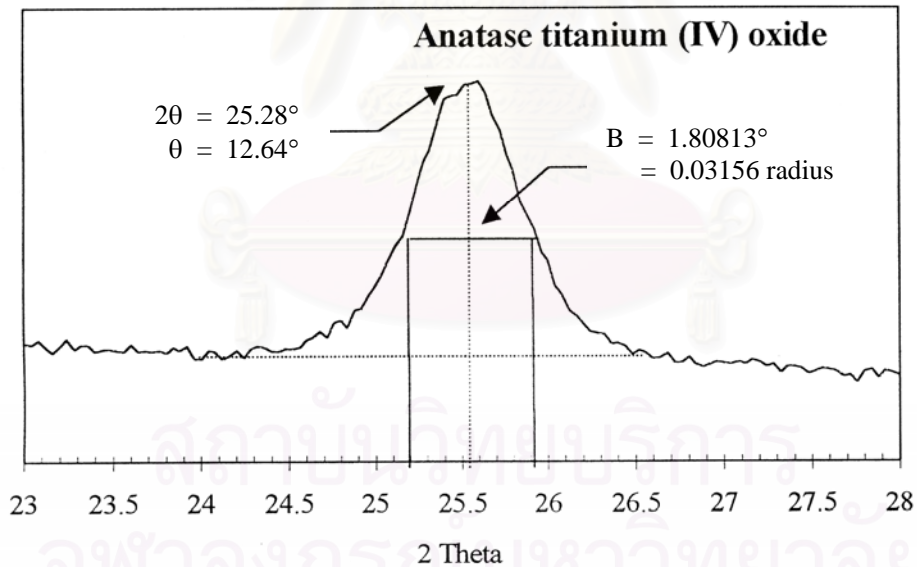


Figure A.1 The 101 diffraction peak of titania for calculation of the crystallite size

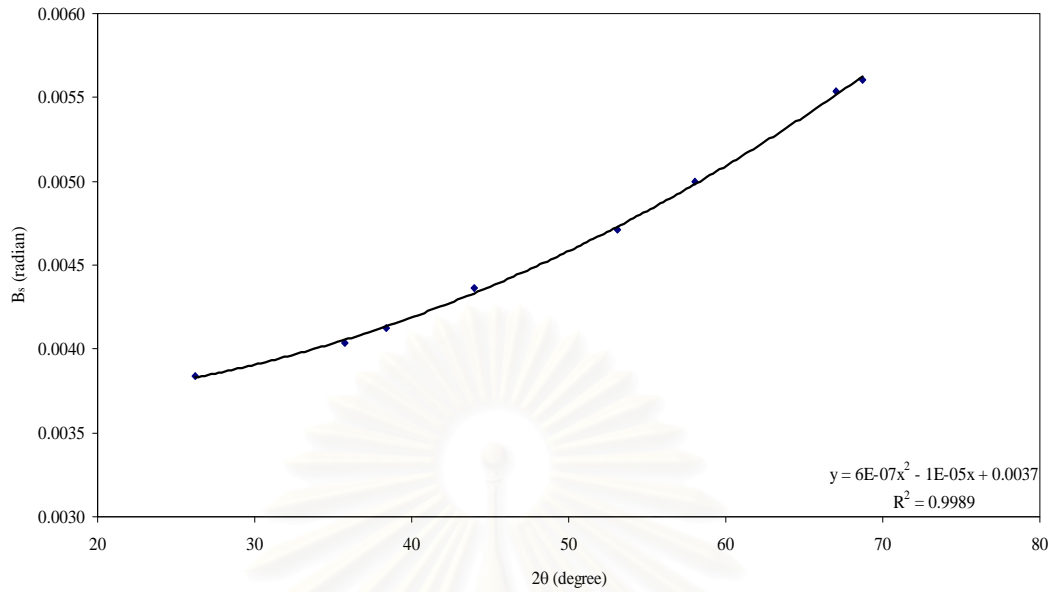


Figure A.2 The plot indicating the value of line broadening due to the equipment. The data were obtained by using α -alumina as standard.

สถาบันวิทยบริการ
จุฬาลงกรณ์มหาวิทยาลัย

APPENDIX B

CALCULATION OF THE CONTACT ANGLE

The contact angle of sample was calculated from height and radius of water droplet using trigonometry formula.

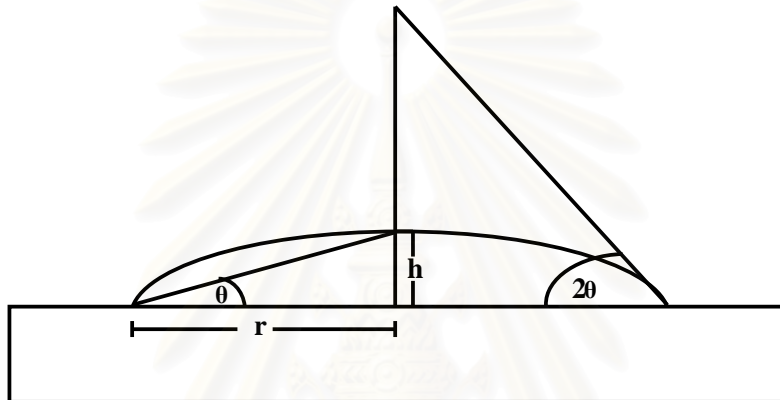


Figure B.1 The shape and dimension of water droplet on the surface.

$$\text{Contact angle} = 2 \arctan \frac{h}{r} \quad (\text{B.1})$$

Where h = water droplet height

r = water droplet radius

2θ = Contact angle

สำนักงานวิทยบริการ
จุฬาลงกรณ์มหาวิทยาลัย

APPENDIX C

DATA AND CALCULATION OF ACID SITE

Table C1 Reported total peak area from Micromeritics Chemisorb 2750

Sample	TPX total peak area
Pure TiO ₂	1.39446
2%ZnO	1.45469
4%ZnO	4.61487
6%ZnO	5.13143
8%ZnO	1.44224
10%ZnO	1.98266
2%ZrO ₂	6.14152
4%ZrO ₂	6.02347
6%ZrO ₂	6.28175
8%ZrO ₂	4.17495
10%ZrO ₂	6.31603
2%Fe ₂ O ₃	1.32512
4%Fe ₂ O ₃	1.47279
6%Fe ₂ O ₃	1.44294
8%Fe ₂ O ₃	1.19345
10%Fe ₂ O ₃	1.6064

Calculation of total acid sites

For pure titania sample, total acid site is calculated from the following steps.

1. Conversion of total peak area to peak volume

Conversion from Micromeritics Chemisorb 2750 is equal 77.5016 ml/area unit.

Therefore, total peak volume is derived from

$$\begin{aligned}
 \text{Total peak volume} &= 77.5016 \times \text{total peak area} \\
 &= 77.5016 \times 1.39446 \\
 &= 108.0729 \text{ ml}
 \end{aligned}$$

2. Calculation for adsorbed volume of 15% NH₃

$$\begin{aligned}
 \text{Adsorbed volume of 15\% NH}_3 &= 0.15 \times \text{total peak volume} \\
 &= 0.15 \times 108.0729 \text{ ml} \\
 &= 16.2109 \text{ ml}
 \end{aligned}$$

3. Calculation of total acid sites

$$\text{Total acid sites} = \frac{(\text{adsorbed volume, ml}) \times 101.325 \text{ Pa}}{(8.314 \times 10^{-3} \frac{\text{Pa} \cdot \text{ml}}{\text{K} \cdot \mu\text{mol}}) \times 298 \text{ K} \times (\text{weight of catalyst, g})}$$

For pure titania sample, 0.1048 g of this sample was measured, therefore

$$\begin{aligned}
 \text{Total acid sites} &= \frac{16.2109 \text{ ml} \times 101.325 \text{ Pa}}{(8.314 \times 10^{-3} \frac{\text{Pa} \cdot \text{ml}}{\text{K} \cdot \mu\text{mol}}) \times 298 \text{ K} \times (0.1048 \text{ g})} \\
 &= 6,326.11 \mu\text{mol H}^+ / \text{g}
 \end{aligned}$$

สถาบันวิทยบริการ
จุฬาลงกรณ์มหาวิทยาลัย

APPENDIX D

DETERMINATION OF Ti^{3+} SURFACE DEFECT FROM ESR MEASUREMENT

The amount of Ti^{3+} surface defect from ESR measurement can be relatively determined from:

$$\text{Ti}^{3+} \text{ surface defects} = \frac{\text{Intensity of ESR peak height}}{(\text{surface area}) \times (\text{catalyst weight})}$$

Example: The Ti^{3+} surface defect of pure titania are determined as follow;

$$\begin{aligned} \text{Ti}^{3+} \text{ surface defect} &= \frac{1,277}{(0.3001 \text{ g}) \times (125.1 \text{ m}^2 \cdot \text{g}^{-1})} \\ &= 34.02 \end{aligned}$$

สถาบันวิทยบริการ
จุฬาลงกรณ์มหาวิทยาลัย

APPENDIX E

DETERMINATION OF LATTICE PARAMETERS OF TITANIUM DIOXIDE

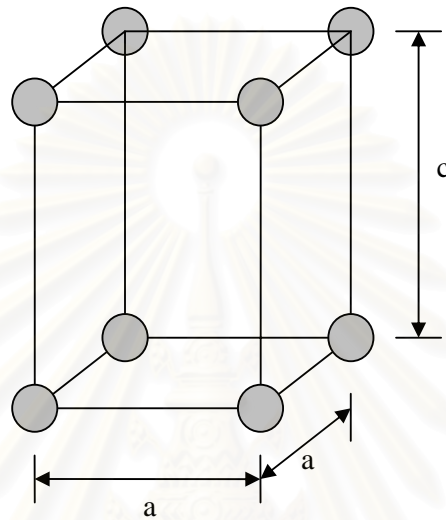


Figure F.1 Tetragonal crystal structure of titanium dioxide

Interplanar spacing (d-spacing) can be calculated from:

$$2d_{hkl} \sin \theta = n\lambda \quad (\text{Bragg's law}) \quad (1)$$

So, at a fixed wavelength (controlled by the XRD machine: target, filter, etc.) for a certain value of d (characteristic of samples). After obtaining the d -spacing of each plane, a -cell and c -cell of lattice parameter can be calculated from:

$$d_{hkl} = \frac{a}{[h^2 + k^2 + l^2 (\frac{a^2}{c^2})]^{1/2}} \quad \text{for tetragonal system} \quad (2)$$

For example, we choose (101) plane and (200) plane of TiO_2 to determine the d -spacing value of each plane

Table F.1 The 2θ value of (101) plane and (200) plane of ZnO/TiO₂ in each sample from XRD measurement

Amount of ZnO (%mol)	2-theta	
	(101) plane	(200) plane
0	25.29°	47.89°
2	25.33°	47.98°
4	25.31°	48.17°
6	25.33°	47.91°
8	25.22°	48.07°
10	25.32°	48.08°

Determination of d-spacing and lattice parameters for pure titania

From Bragg's law
$$d_{hkl} = \frac{n\lambda}{2\sin\theta} \quad (3)$$

Where $n = 1$ and λ for CuK $\alpha = 1.54439 \text{ \AA}$

Substituting n , λ and θ into equation (3), we obtain

$$d_{101} = \frac{(1)(1.54439)}{(2)[\sin(25.29/2)]} = 3.5280 \text{ \AA}$$

$$d_{200} = \frac{(1)(1.54439)}{(2)[\sin(47.89/2)]} = 1.9026 \text{ \AA}$$

The d-spacing of (200) plane is used to determine a-cell parameter;

$$a = (2)(d_{200}) = (2)(1.9026) = 3.8053 \text{ \AA} \quad (4)$$

And c-cell parameter can be determined from Equation (5) below.

$$c = \left(-\frac{(d_{101})^2 (a)^2}{((d_{101})^2 - (a)^2)} \right)^{1/2} \quad (5)$$

$$= \left(-\frac{(3.5280)^2 (3.8053)^2}{((3.5280)^2 - (3.8053)^2)} \right)^{1/2} = 9.4136 \text{ \AA}$$

The crystal volume of TiO₂ can be calculated from:

$$\begin{aligned} \text{Crystal volume of anatase TiO}_2 &= (a)^2(c) \quad (6) \\ &= (3.8053)^2(9.4136) = 136.312 \text{ \AA}^3 \end{aligned}$$

Table F.2 Summary of lattice parameters and crystal volume from XRD analysis

Sample	d ₁₀₁ (\AA)	d ₂₀₀ (\AA)	a-cell parameter (\AA)	c-cell parameter (\AA)	Crystal volume (\AA ³)
Pure TiO ₂	3.5280	1.9026	3.8053	9.4136	136.3116
2%ZnO	3.5216	1.8989	3.7978	9.4061	135.6681
4%ZnO	3.5250	1.8922	3.7845	9.6867	138.7357
6%ZnO	3.5225	1.9019	3.8038	9.3339	135.0521
8%ZnO	3.5371	1.8960	3.7919	9.8140	141.1116
10%ZnO	3.5236	1.8956	3.7912	9.5486	137.2410
2%ZrO ₂	3.5292	1.8981	3.7963	9.5789	138.0493
4%ZrO ₂	3.5125	1.8969	3.7938	9.2954	133.7896
6%ZrO ₂	3.5148	1.8940	3.7880	9.4251	135.2419
8%ZrO ₂	3.5174	1.8944	3.7888	9.4640	135.8556
10%ZrO ₂	3.5278	1.9026	3.8053	9.4112	136.2762
2%Fe ₂ O ₃	3.5244	1.8999	3.7998	9.4293	136.1451
4%Fe ₂ O ₃	3.5229	1.9018	3.8035	9.3456	135.2023
6%Fe ₂ O ₃	3.5289	1.9092	3.8184	9.2397	134.7138
8%Fe ₂ O ₃	3.5240	1.8996	3.7991	9.4324	136.1400
10%Fe ₂ O ₃	3.5220	1.9107	3.8215	9.0758	132.5391

LIST OF PUBLICATIONS

Natapong Sonsa-ard, Akawat Sirisuk. “Effect of addition of second metal oxide on hydrophilic property of TiO₂ thin film”, Pure and Applied Chemistry International Conference 2008, Bangkok, Thailand, January 30- February 1, 2008.



สถาบันวิทยบริการ
จุฬาลงกรณ์มหาวิทยาลัย

VITA

Mr. Natapong Sonsa-ard was born on March 5, 1984 in Chonburi province, Thailand. He received the Bachelor Degree of Chemical Engineering from Faculty of Engineering, Burapha University, in 2006. He pursued his Master's study at Chulalongkorn University in June, 2007.



สถาบันวิทยบริการ
จุฬาลงกรณ์มหาวิทยาลัย